DOE/ER60894-4

SPECT ASSAY OF RADIOLABELED MONOCLONAL ANTIBODIES

DOE/ER/60894--4

DE92 019915

COMPREHENSIVE PROGRESS REPORT

SEPTEMBER 1989 - FEBRUARY 1992

Ronald J. Jaszczak

Radiology Department

Duke University Medical Center

Durham, North Carolina 27710

DISCLAIMER

February 1992

PREPARED FOR THE U.S. DEPARTMENT OF ENERGY
UNDER GRANT NUMBER DE-FG05-89ER60894

A. TABLE OF CONTENTS

Page

B. INTRODUCTION

This application represents the continuation of a grant funded initially in September, 1989. The long-term goal of this research project is to develop methods to improve the utility of single photon emission computed tomography (SPECT) to quantify the biodistribution of monoclonal antibodies (MoAbs) labeled with clinically relevant radionuclides (^{123}I, ^{131}I, and ^{111}In) and with another radionuclide,^{211}At, recently used in therapy. In the following sections, we describe our progress in developing quantitative SPECT methodology for ^{111}In and ^{123}I. We also present selected preliminary studies directed towards attaining the specific aims for the next project period. Additional research results for this project and for complementary Duke research projects relating to SPECT and radiolabeled MoAbs are summarized in the listed publications.

We have focused our research thrusts on the following aspects of SPECT: 1) The development of improved SPECT hardware, such as improved acquisition geometries. 2) The development of better reconstruction methods that provide accurate compensation for the physical factors that affect SPECT quantification. 3) The application of carefully designed simulations and experiments to validate our hardware and software approaches.

We recognize that this effort involves several areas of research; however, we believe that these research areas complement each other and form a well-integrated approach to improving SPECT quantification.

C. PRINCIPAL RESEARCH ACCOMPLISHMENTS (SEPTEMBER 1989-FEBRUARY 1992)

1. Implementation of two-dimensional (2D) versions of filtered backprojection (FBP) and maximum likelihood-expectation maximization (ML-EM) algorithms which compensate for non-uniform attenuation, detector response, and scatter.

2. Determination of accuracy, bias, and signal-to-noise ratios of these algorithms for ^{123}I and ^{111}In using simulated and experimentally acquired phantom data.

3. Development of parallel beam and fan beam geometries to obtain transmission computed tomographic (TCT) data to be used to determine attenuation maps for non-uniform attenuation compensation in SPECT.

4. Determination of the accuracy to register SPECT, PET, and MRI images that can be attained with the surface fitting method of Pellizari et al [1989], using a 3D brain phantom and patient scans.

5. Preliminary investigation of pinhole SPECT imaging using Monte Carlo simulated projection data and a modified cone-beam FBP algorithm.

6. Preliminary investigation of the feasibility of SPECT to image ^{211}At within isolated source distributions using experimentally acquired data.

D. PUBLICATIONS

Since this is the first Project Period of this grant, the publications listed below only include articles that were published during the two and one-third-year period September 1989 through January 1992.

D.1. JOURNAL ARTICLES, CHAPTERS, AND PUBLISHED PROCEEDINGS

1. Gilland DR, Jaszczak RJ, Greer KL, Coleman RE: Quantitative SPECT reconstruction of Iodine-123 Data. J Nucl Med 32:527-533, 1991a.

2. Gilland DR, Jaszczak RJ, Turkington TG, Greer KL, Coleman RE: Quantitative SPECT imaging with Indium-111. IEEE Trans Nucl Sci 38:761-766, 1991b.

3. Jaszczak RJ, Hoffman DC: Variance propagation for SPECT with energy-weighted acquisition. IEEE Trans Nucl Sci 38:739-747, 1991.

4. Jaszczak RJ: SPECT: State-of-the-art scanners and reconstruction strategies. In: *Radiopharmaceuticals and Brain Pathology Studied with PET and SPECT*. Ed. M. Diksic and R.C. Reba (CRC Press, 1990), pp. 93-118.

5. Gilland DR, Jaszczak RJ, Turkington TG: Quantitative SPECT imaging with indium-111. In: *Conference Record of the 1990 IEEE Nuclear Science Symposium* (Arlington, VA, Dibler, 1990), pp. 1194-1199.

6. Jaszczak RJ, Hoffman DC, DeVito RP: Variance propagation for SPECT with energy-weighted acquisition. In: *Conference Record of the 1990 IEEE Nuclear Science Symposium* (Arlington, VA, Dibler, 1990), pp. 1163-1171.

7. Jaszczak RJ, Li J, Wang H, Greer KL, Coleman RE: Three dimensional reconstruction of combined cone beam and parallel beam data. Phys Med Biol, in press, 1992.

8. Gilland DR, Tsui BW, Metz CE, Jaszczak RJ, Perry R: An evaluation of maximum likelihood EM reconstruction by ROC analysis: J Nucl Med, in press, 1992.

9. Gilland DR, Jaszczak RJ, Liang Z, Greer KL, Coleman RE: Quantitative SPECT brain imaging: Effects of attenuation and collimator response. IEEE Trans Nucl Sci, submitted, 1992.

10. Turkington TG, Jaszczak RJ, Greer KL, Coleman RE: Correlation of SPECT images of a three-dimensional brain phantom using a surface fitting technique. IEEE Trans Nucl Sci, submitted, 1992.

11. Gilland DR, Jaszczak RJ, Greer KL, Coleman RE: SPECT quality control: Generation and reduction of artifacts. In: *Proceedings of the SE Chapter of the Society of Nuclear Medicine*, in press, 1992.

12. Gilland DR, Jaszczak RJ, Liang Z, Greer KL, Coleman RE: Quantitative SPECT brain imaging: Effects of attenuation and collimator response. In: *Conference Record of the 1991 IEEE Nuclear Science Symposium (Santa Fe, NM, 1991)* in press.

13. Turkington TG, Jaszczak RJ, Greer KL, Coleman RE: Correlation of SPECT images of three-dimensional brain phantom using a surface fitting technique. In: *Conference Record of the 1991*

IEEE Nuclear Science Symposium (Santa Fe, NM, 1991b) in press.

14. Jaszczak RJ, Tsui BMW: Single photon emission computed tomography, In: *Principles of Nuclear Medicine*, eds. H. Wagner and Z. Szabo (W.B. Saunders, Philadelphia, 1993), in preparation.

15. Jaszczak RJ, Hoffman EJ: Scatter and attenuation in SPECT and PET, In: *Principles of Nuclear Medicine*, eds. H. Wagner and Z. Szabo (W.B. Saunders, Philadelphia, 1993), in preparation.

D.2. ABSTRACTS

16. Gilland DR, Jaszczak RJ, Greer KL, Zalutsky MR, Coleman RE: SPECT quantification with Iodine-123. J Nucl Med 31(5): 874 (Abstract), 1990.

17. Turkington TG, Jaszczak RJ, Gilland DR, Greer KL, Coleman RE: Quantitation of Indium-111 activity in SPECT. J Nucl Med 32(5):986 (Abstract), 1991a.

18. Gilland DR, Jaszczak RJ, Coleman RE: Effects of non-uniform attenuation compensation in SPECT using acquired transmission data. J Nucl Med 32(5):1067, (Abstract), 1991c.

19. Turkington TG, Jaszczak RJ, Pelizzari CA, Harris CC, MacFall JR, Hoffman JM: Measurement of accuracy in registration of PET and SPECT brain images to MR images. Radiology 181(P): 186, (Abstract), 1991c.

20. Jaszczak RJ, Li J, Wang H, Coleman RE: SPECT collimation having spatially variant focusing (SVF). Society of Nuclear Medicine 39th Annual Meeting (Abstract), Los Angeles, June 1992, accepted.

21. Gilland DR, Jaszczak RJ, Turkington TG, Greer KL, Coleman RE: Transmission data acquisition with a three headed SPECT system. Society of Nuclear Medicine 39th Annual Meeting (Abstract), Los Angeles, June 1992, accepted.

22. Gilland DR, Bowsher JE, Jaszczak RJ, Coleman RE: Improved signal-to-noise with 3D ML-EM reconstruction. Society of Nuclear Medicine 39th Annual Meeting (Abstract), Los Angeles, June 1992, accepted.

23. Turkington TG, Jaszczak RJ, Hoffman JM, MacFall JR, Harris CC, Kilts CD, Pelizzari CA, Coleman RE: Accuracy of surface fit registration of PET and MR brain images. Society of Nuclear Medicine 39th Annual Meeting (Abstract), Los Angeles, June 1992, accepted.

24. Bowsher JE, Gilland DR, Floyd CE, Jaszczak RJ, Johnson VE, Coleman RE: Three-dimensional iterative reconstruction for SPECT. Society of Nuclear Medicine 39th Annual Meeting (Abstract), Los Angeles, June 1992, accepted (Selected as one of six finalist papers for SNM Young Investigators Award Session at SNM Annual Meeting to be held in Los Angeles, June, 1992).

D.3. RELATED PUBLICATIONS SUPPORTED IN PART BY DOE GRANT DE-FG05-91ER60894

25. Manglos SH, Jaszczak RJ, McAfee JG: Maximum likelihood reconstruction for cone beam SPECT with camera tilt. IEEE Trans Nucl Sci NS36:1117-1121, 1989.

26. Manglos SH, Jaszczak RJ, Greer KL: Cone beam SPECT reconstruction with camera tilt. Phys Med Biol 34:625-631, 1989.

27. Liang Z, Jaszczak RJ: On Bayesian image reconstruction from projections: Uniform and non-uniform *a priori* source information. IEEE Trans Med Imaging 8:227-235, 1989.

28. Manglos SH, Jaszczak RJ, Floyd CE: Maximum likelihood reconstruction for cone beam SPECT: development and initial tests. Phys Med Biol 34:1947-1957, 1989.

29. Liang Z, Jaszczak RJ, Floyd CE, Greer KL, Coleman RE: Bayesian reconstruction for SPECT: Validation with Monte Carlo simulation, experimental phantom, and real patient data. International Journal of Imaging Systems and Technology 1:149-168, 1989.

30. Liang Z, Jaszczak RJ: Comparisons of multiple photon coincidence imaging techniques. IEEE Trans on Nucl Science 37:1282-1292, 1990.

31. Liang Z, Jaszczak RJ, Coleman RE, Johnson V: Simultaneous reconstruction, segmentation, and edge enhancement of piecewise continuous images with intensity-level information. Med Phys 18:394-401, 1991.

32. Zasadny KR, Koral KF, Floyd CE, Jaszczak RJ: Measurement of Compton scattering in phantoms by germanium detector. IEEE Trans on Nucl Science 37:642-646, 1990.

33. Wang X, Koral KF, Clinthorne NH, Rogers WL, Floyd CE, Jaszczak RJ: Effect of noise, order and range in fitting the photopeak region of local, Anger-camera spectra. Nuclear Instruments and Methods in Physics Research A299:548-553, 1990.

34. Koral KF, Wang X, Zasadny KR, Clinthorne NH, Rogers WL, Floyd CE, Jaszczak RJ: Testing of local gamma-ray scatter fractions determined by spectral fitting. Phys Med Biol 36:177-190, 1991.

35. Cope DA, Dewhirst MW, Friedman HS, Bigner DD, Zalutsky MR: Enhanced delivery of a monoclonal antibody F(ab')2 fragment to subcutaneous human glioma xenografts using local hyperthermia. Cancer Res. 50:1803-1809, 1990.

36. Garg PK, Harrison CL, Zalutsky MR: Comparative tissue distribution in mice of the a-emitter ^{211}At and ^{131}I as labels of a monoclonal antibody and F(ab')2 fragment. Cancer Res 50:3514-3520, 1990.

37 Liang Z, Jaszczak RJ, Floyd CE, Greer KL, Coleman RE: Reprojection and backprojection in SPECT image reconstruction. In: *Proceedings of the Southeastcom '89 Conference on Energy and Information Technologies in the Southeast* (Columbia, SC, April 9-12, 1989), IEEE-CH2674, 1989, pp. 919-926.

38. Coleman RE, Jaszczak RJ, Greer KL,Mercer RR, Crapo, JD: Regional dosimetry of inhaled particles using SPECT. In: *Extrapolation of Dosimetric Relationships for Inhaled Particles and Gases*, Eds. JD Crapo, ED Smolko, FJ Miller, JA Graham, AW Hayes (Academic Press, Sad Diego, 1989) pp. 201-210.

39. Smith MF, Jaszczak RJ, Floyd CE, Greer KL, Coleman RE: Interactive visualization of three-dimensional SPECT cardiac images. In: *Proceedings of the Third Annual IEEE Symposium on*

Computer-Based Medical Systems. (Chapel Hill, North Carolina, June 3-8, 1990), pp. 213-219.

40. Smith MF, Floyd CE, Jaszczak RJ, Coleman RE: Reconstruction of SPECT Images using Generalized Matrix Inverses. In: *Conference Record of the 1990 IEEE Nuclear Science Symposium* (Arlington, VA, Dibler, 1990), pp. 1487-1497.

41. Liang Z, Gilland D, Jaszczak R, Coleman R: Implementation of non-linear filters for iterative maximum likelihood image reconstruction. In: *Conference Record of the 1990 IEEE Nuclear Science Symposium* (Arlington, VA, Dibler, 1990), pp. 1518-1522.

42. Liang Z, Jaszczak R: Discussion of the paper by Silverman, Jones, Wilson and Nychko, J Royal Statist Soc 52(2): 317, 1990.

43. Liang Z, Jaszczak R, Floyd C, Greer K: A spatial interaction model for statistical image processing. In: *Information Processing in Medical Imaging*, eds D.A. Ortendahl, J Llacer (Wiley-Liss, New York, 1990) pp. 29-43.

44. Garg PK, Bigner DD, Zalutsky MR: Enhancing tumor dose via improved antibody radiohalogenation and alpha-emitting astatine-211. In: *Epenetos AA (Ed.) Advances in the Applications of Monoclonal Antibodies in Clinical Oncology* (Chapman and Hall) 1991, pp. 101-112.

45. Liang Z, Jaszczak R, Coleman R: On reconstruction and segmentation of piecewise continuous images. In: *Information Processing in Medical Imaging, 12th International Conference* (Springer-Verlag, Berlin, 1991), pp. 94-104.

46. Smith MF, Floyd CE, Jaszczak RJ, Coleman RE: Reconstruction of SPECT images using generalized matrix inverses. IEEE Trans Med Imaging, in press, 1992.

47. Smith M, Floyd C, Jaszczak R, Coleman R: Three dimensional photon detection kernels and their application to SPECT reconstruction. Phys Med Biol, in press, 1992.

48. Liang Z, Turkington TG, Gilland DR, Jaszczak RJ, Coleman RE: Simultaneous compensation for attenuation, scatter, and detector response for SPECT reconstruction in three dimensions. Phys Med Biol, in press, 1992.

49. Wang H, Jaszczak RJ, Coleman RE: Solid geometry based object model for Monte Carlo simulated emission and transmission tomographic imaging systems. IEEE Trans Med Imaging, in press, 1992.

50. Li J, Jaszczak RJ, Greer KL, Coleman RE: Experimental evaluation of combined cone beam with parallel hole collimation SPECT data. In: *Conference Record of the 1991 IEEE Nuclear Science Symposium* (Santa Fe, NM 1991), in press.

51. Liang Z, Jaszczak R, Coleman R: An efficient 3D unified projector-backprojector for SPECT reconstruction. In: *Conference Record of the 1991 IEEE Nuclear Science Symposium* (Santa Fe, NM 1991), in press.

52. Wang H, Jaszczak RJ, Gilland DR, Greer KL, Coleman RE: Solid geometry based modeling of non-uniform attenuation and Compton scattering in objects for SPECT imaging systems. In: *Conference Record of the 1991 IEEE Nuclear Science Symposium* (Santa Fe, NM 1991), in press.

53. Smith MF, Floyd CE, Jaszczak RJ, Coleman RE: Evaluation of projection pixel-dependent and pixel-independent scatter correction in SPECT. In: *Conference Record of the 1991 IEEE Nuclear Science Symposium* (Santa Fe, NM 1991), in press.

54. Li J, Jaszczak RJ, Greer KL, Coleman RE: Experimental evaluation of combined cone beam with parallel hole collimation SPECT data. IEEE Trans Nucl Sci, submitted, 1992.

55. Liang Z, Jaszczak RJ, Coleman RE: An efficient 3D unified projector-backprojector for SPECT reconstruction. IEEE Trans Nucl Sci, submitted, 1992.

56. Smith MF, Floyd CE, Jaszczak RJ, Coleman RE: Evaluation of projection pixel-dependent and pixel-independent scatter correction in SPECT. IEEE Trans Nucl Sci, submitted, 1992.

57. Wang H, Jaszczak RJ, Gilland DR, Greer KL, Coleman RE: Solid geometry based modeling of non-uniform attenuation and Compton scattering in objects for SPECT imaging systems. IEEE Trans Nucl Sci, submitted, 1992.

58. Leichner PK, Koral KF, Jaszczak RJ, Green AJ, Chen G, Roeske JC: Imaging techniques and treatment planning in radioimmunotherapy (RIT): Med Phys, submitted, 1992.

59. Schold SC, Zalutsky MR, Glantz MJ, Coleman RE, Friedman AH, Jaszczak RJ, Bigner SH, Bigner DD: Distribution and dosimetry of 123-I labeled monoclonal antibody 81C6 in patients with anaplastic glioma. Invest Radiology, submitted, 1992.

D.4. Abstracts Supported in Part by DOE Grant Number DE-FG05-91ER60894

60. Liang Z, Jaszczak RJ, Floyd CE, Greer KL, Coleman RE: Validation of Bayesian reconstruction with Monte Carlo simulations and real data. J Nucl Med 30(5):755 (Abstract), 1989.

61. Mendez GE, Jaszczak RJ, Greer KL, Gilland DR, Coleman RE: ROC evaluation of cone beam and parallel beam collimators. J Nucl Med 31(5):718 (Abstract), 1990.

62. Liang Z, Jaszczak R, Coleman R: Simultaneous reconstruction, segmentation, and edge enhancement of simulated heart images using a multinomial model and concentration-level information. J Nucl Med 31(5): 858 (Abstract), 1990.

63. Smith MF, Jaszczak RJ, Floyd CE, Greer KL, Coleman RE: Evaluation of SPECT images using interactive three-dimensional display. J Nucl Med 31(5):807 (Abstract), 1990.

64. Smith MF, Floyd CE, Jaszczak RJ, Coleman RE: Reconstructing SPECT images using three-dimensional photon detection kernels. J Nucl Med 32(5):1068 (Abstract), 1991.

65. Liang Z, Jaszczak RJ, Coleman RE: A 3D model for simultaneous compensation of non-uniform attenuation and collimation divergence of SPECT image reconstruction. J Nucl Med 32(5): 917 (Abstract), 1991.

66. Wang H, Jaszczak RJ, Coleman RE: Monte Carlo model of non-uniform attenuating phantoms with irregular-shaped regions for SPECT imaging systems. J Nucl Med 32(5):1065, (Abstract), 1991.

67. Li J, Jaszczak RJ, Wang H, Greer KL, Coleman R: Evaluation of combined cone beam with parallel hole collimation SPECT data. J Nucl Med 32(5):956, (Abstract), 1991.

68. Li J, Wang H, Jaszczak RJ, Coleman RE: A cone beam reconstruction algorithm with a displaced center-of-rotation. Society of Nuclear Medicine 39th Annual Meeting, (Abstract), Los Angeles, June 1992, accepted.

69. Liang Z, Coleman RE: Restoration for detector response in high resolution PET image reconstruction. Society of Nuclear Medicine 39th Annual Meeting (Abstract), Los Angeles, June, 1992, accepted.

70. Zeng GL, Gullberg GT, Jaszczak RJ, Li J: Fan beam convolution reconstruction algorithms for variable focal length collimators. Abstract submitted to the Society of Nuclear Medicine 39th Annual Meeting (Abstract), Los Angeles, June 1992, accepted.

D.5. Related Publications Supported by Prof. Zalutsky's DOE Grant (DE-FG5-89ER60789)

71. Vaidyanathan G, Zalutsky MR: Radioiodination of antibodies via N-succinimidyl 2,4-dimethoxy-3-(trialkylstannyl)benzoates. Bioconjugate Chem 1:387-393, 1990.

72. Zalutsky MR, Garg PK, Narula AS: Labeling monoclonal antibodies with halogen nuclides. Acta Radiol Suppl 374, 1990.

73. Garg PK, Garg S, Zalutsky MR: Fluorine-18 labeling of monoclonal antibodies and fragments with preservation of immunoreactivity. Bioconjugate Chem 2:50-56, 1991.

74. Garg S, Garg PK, Zalutsky MR: N-succinimidyl 5-(trialkylstannyl)-3-pyridinecarboxylates: A new class of reagents for protein radioiodination. Bioconjugate Chem 2:50-56, 1991.

75. Garg PK, Garg S, DeGraff WG, Zalutsky MR, Mitchell JB: 4-Fluorobenzylamine and phenylalanine methyl ester conjugates of 2-nitroimidazole: evaluation as hypoxic cell radiosensitizers. Int J Radiat Oncol Biol Phys, in press, 1992.

76. Vaidyanathan G, Zalutsky MR: Labeling proteins with fluorine-18 using N-succinimidyl 4-[18F] fluorobenzoate. Nucl Med Biol, in press, 1992.

77. Zalutsky MR, Garg PK, Vaidyanathan G, Garg S: Methods for the radiohalogenation of antibodies. In: *Applications for Enzyme Biotechnology*, Plenum Press, in press, 1992.

78. Zalutsky MR, Garg PK, Johnson SH, Coleman RE: Fluorine-18 antimyosin monoclonal antibody fragments: Preliminary investigation in a canine myocardial infarct model. J Nucl Med, submitted, 1992.

79. Garg S, Garg PK, Bigner DD, Zalutsky MR: Selective localization of an 18F labeled Mel-14 monoclonal antibody $F(ab')_2$ fragment in a subcutaneous human glioma xenograft model, J Nucl Med, submitted, 1992.

80. Schuster JM, Dewhirst MW, Bigner DD, Zalutsky MR: Distribution of radiolabeled monoclonal antibody F(ab')$_2$ fragments in a subcutaneous xenograft model following localized hyperthermia: Temperature effects, Int. J Radiat Oncol Biol Phys, submitted, 1992.

81. Vaidyanathan G, Bigner DD, Zalutsky MR: Fluorine-18 labeled monoclonal antibody fragments: A potential approach for combining radioimmunoscintigraphy and positron emission tomography, Cancer Res, submitted, 1992.

E. Principal Project Personnel and Graduate Training

E.1. Principal Project Personnel

E.1.1. Ronald J. Jaszczak (25%), Ph.D.

Dr. Jaszczak is a Professor of Radiology, a Professor of Biomedical Engineering, and a Research Professor in the Institute of Statistics and Decision Sciences (ISDS). Prof. Jaszczak is the Principal Investigator for this grant, and has overall administrative and scientific responsibility for the project. He is actively involved in all areas of the work, particularly in evaluating and debugging simulation and reconstruction software, collecting and analyzing experimentally acquired SPECT data, ensuring proper performance of the triple-camera research SPECT system, and preparing published articles and reports. Prof. Jaszczak's level of effort is 25%.

E.1.2. David Gilland (100%), Ph.D.

Dr. Gilland is a Research Associate in Radiology and has extensive experience in the area of SPECT. His Ph.D. dissertation involved the evaluation of iterative SPECT reconstruction algorithms using receiver operator characteristics (ROC) methodology. He has performed simulations and experiments to evaluate the capability of SPECT to quantify ^{123}I and ^{111}In. He is responsible for developing accurate physical models of the probability matrices that will be used in the statistical Bayesian reconstruction algorithms. He has worked closely with Prof. Jaszczak in implementing computational efficient 3D reconstruction algorithms for imaging radiolabeled MoAbs. He is responsible for the evaluation of these algorithms. Dr. Gilland's level of effort on this project is 100%.

E.1.3. Timothy Turkington (75%), Ph.D.

Dr. Turkington is a Research Associate in Radiology and has led our effort in developing our custom 3D SPECT image processing software package ("SPECTER"), which is used by several groups of investigators in Radiology. He has also implemented and determined the accuracy of a surface-fitting method to register SPECT, PET and MRI images. Several research groups in Radiology are using this software package. He has performed experiments to evaluate the capability of SPECT to measure *in vitro* and *in vivo* distributions of MoAbs labeled with ^{123}I, ^{111}In, and ^{211}At. Dr. Turkington's level of effort on this project is 75%.

E.1.4. Jiang Qian (50%), M.S.

Ms. Qian is a Graduate Student in the Institute of Statistics and Decision Sciences (ISDS). She joined this project in January, 1992, and she will be responsible for implementing and evaluating 3D Bayesian reconstruction algorithms. She will work closely with Profs. Jaszczak and Valen Johnson (see E.2.2) and with Dr. Gilland to ensure that the SPECT acquisition process is accurately modeled and that the algorithms are computationally efficient. Effective January, 1992, Ms. Qian's level of effort on this project is 50%.

E.1.5. Kim L. Greer (17%), N.M.T.

Mr. Greer is the SPECT Research Technologist. He works closely with the investigators in experimentally acquiring SPECT data using the Triple-Camera Research SPECT system. He is responsible for transferring data between this system and other SPECT computer facilities. He reconstructs SPECT images and analyzes 3D SPECT data in collaboration with the investigators of this project. He is responsible for ensuring that the Research SPECT system and SPECT laboratory computers are maintained properly, and that these facilities are used efficiently. He designs and builds some of the fixtures and mechanical devices required for the acquisition of experimental data. Mr. Greer's level of effort on this project is 17%.

E.2. Faculty Associates and Consultants

E.2.1. R. Edward Coleman, M.D.

Dr. Coleman is Director of Nuclear Medicine at Duke University Medical Center. Dr. Coleman also directs the PET facility at Duke and has participated in multiple projects as a clinical investigator. Dr. Coleman is a faculty associate on this grant. He will assist in the design of experimental studies, and serve as a consultant to ensure that all medically oriented objectives are appropriate. No funds are requested to support Dr. Coleman's effort on this project.

E.2.2. Valen Johnson, Ph.D.

Dr. Johnson is an Assistant Professor in the Institute of Statistics and Decision Sciences. Prof. Johnson will serve as a faculty associate in the area of statistical reconstruction algorithms. He is developing appropriate statistical models for Emission Computed Tomography (ECT). He is a consultant on this project to ensure that our physical models are integrated within an appropriate statistical model. Prof. Johnson will co-direct, with Prof. Jaszczak, the Graduate Student, Ms. Jiang Qian, who is responsible for implementing the Bayesian reconstruction algorithm. No funds are requested to support Prof. Johnson's effort on this project.

E.2.3. Michael Zalutsky, Ph.D.

Dr. Zalutsky is a Professor of Radiology and is a Principal Investigator of DOE and NIH research projects directed towards the development of new radiolabeled MoAbs. Prof. Zalutsky is a faculty associate in the area of radiochemistry, and will assist in the design of experimental studies. He is a consultant to ensure that these studies appropriately address problems that are significant in the development and evaluation of new MoAbs. No funds are requested to support Prof. Zalutsky's effort on this project.

F. Training

F.1. Undergraduate, Graduate, and Post-Doctoral Training

Although the Department of Radiology does not have a non-medical graduate program , undergraduate and graduate students from the Department of Biomedical Engineering (BME) and the Institute of Statistics and Decision Sciences (ISDS) have worked in our SPECT research laboratory. For example, a BME undergraduate student, Robert Herstein, did an independent research project in the laboratory during his senior year. This SPECT project was used to support his application for Graduation with Distinction. David Hoffman from BME recently performed M.S. thesis research in our SPECT laboratory. Another BME graduate student, Randy Capone, spent last year with us, and was recently awarded his M.S. degree. He is now in the process of applying to medical school. Presently there are two graduate students being trained in our SPECT laboratory. One of these students, Ms. Jiang Qian, is being supported in part (50%) by this DOE grant. Ms. Qian is a second year graduate student in ISDS, and her faculty advisor is Professor Valen Johnson. The second student, Mr. Sunyang Jang, is a first year graduate student in the Department of Biomedical Engineering (BME). Mr. Jang will be supported in part by an NIH grant (CA33541). Prof. Jaszczak is Mr. Jang's faculty advisor. Furthermore, Mark Smith, Ph.D., has a Post-doctoral Fellowship supported by the National Institutes of Health, and his research is being performed in our SPECT laboratory.

G. Development of SPECT Software

G.1. Quantitative SPECT Imaging Using Three-Dimensional ML-EM Algoritpm

The maximum likelihood-expectation maximization (ML-EM) algorithm [Shepp and Vardi 1982, Lange and Carson 1984] used in previous work [Gilland 1991a,b] treated SPECT reconstruction as a two-dimensional problem. Thus, inter-slice effects were not considered. It has been shown, however, that inter-slice effects can be significant. For example, for a 11.3 cm radius cylinder, filled uniformly with Tc-99m solution, a 0.45 cm slice thickness, and a general purpose collimator, approximately one third of all non-scatter photons detected within a given slice originate from other slices [Munley et al 1991, Smith et al 1992]. Approximately 23% of all detected photons have scattered and 83% of these photons are from other slices.

G.1.1. Methods

In order to model the three-dimensional (3D) nature of the detector response, a new 3D ML-EM algorithm was designed and implemented. The algorithm was designed for maximal computational speed while staying within the memory limitations of modern workstations. At the heart of the algorithm is the specification of the detection probabilities. It is here that the physical effects of detector response and attenuation are modeled. The divergent nature of the detector response and only uniform attenuation are considered. ***We will extend this to non-uniform attenuation in the next project period.***

In the design of any algorithm such as this, there tends to be a trade-off between computational time and memory requirements. However, in the design of this algorithm a number of steps were taken to maximize speed without impractical memory requirements. First of all, the only source voxels which are reconstructed are those which have been determined *a priori* to be possibly-active, or to possibly contain non-negligible radioactivity concentration; thus, no time is wasted reconstructing empty voxels. Secondly, the detection probability from each source voxel to each projection bin is pre-computed prior to the first ML-EM iteration, rather than re-computed at each iteration, resulting in a substantial time savings. Two factors help to reduce the memory requirements of the "pre-compute" approach. First, by reconstructing only possibly-active voxels no memory is wasted on empty voxels. Second, a single attenuation probability is assumed for all photons emitted from a given voxel and registered at a given detector angle. This is the approximate attenuation probability for the central ray of the collimator's acceptance cone for the source voxel of interest.

The 3D ML-EM algorithm was compared with the filtered backprojection method (FBP) in terms of the signal-to-noise ratio (SNR) in the reconstructed image. The methods were tested on simulated projection data of an elliptical cylinder with uniform activity except for two spherical lesions with 50% decreased activity. The lesions were 2 cm in diameter and located on and 7 cm off the axis of rotation. An ensemble of 10 projection data sets were simulated incorporating the effects of 3D distance-dependent detector response, attenuation, and Poisson noise. The total counts/(0.36 cm thick slice) were 675,000. Lesion contrast, defined as mean background counts minus mean lesion counts divided by mean background counts, was computed using a 1.5 cm diameter circular ROI at the known lesion location. The signal-to-noise ratio was computed in the slice through the lesion center as the average lesion contrast divided by the standard deviation of lesion contrast over the 10 reconstructed images. The ML-EM algorithm was tested at 10, 25, 50 and 100 iterations. The FBP method employed Chang attenuation

compensation (one iteration) and a Metz filter (powers 2, 6, and 12) for detector response compensation.

G.1.2. Results

For both lesion locations, the ML-EM method had better SNR than the FBP method for nearly all of the reconstruction parameters tested (Figure 1). For the off axis lesion, for example, the ML-EM SNR was 31.4 at 50 iterations compared with 19.6 and 15.7 for the FBP with Metz filter powers of 2 and 6, respectively. Thus, a substantial improvement in SNR can be achieved with the 3D ML-EM method compared to FBP. Through efficient implementation of the 3D ML-EM algorithm the reconstruction time per iteration for a 16x24x12 cm volume with a 0.36 cm linear sampling interval is approximately 7.5 minutes on a SUN SPARCstation II.

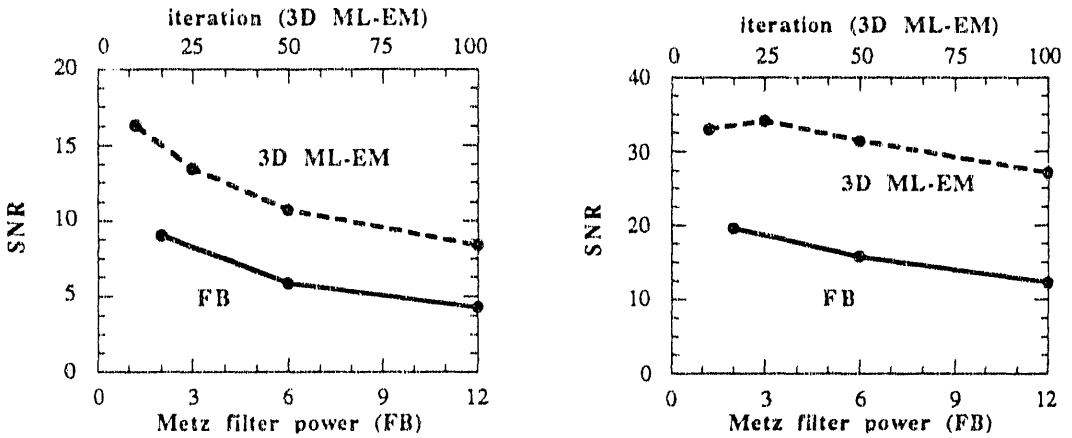

(a) On axis lesion (b) Off axis lesion

Figure 1. Signal-to-noise measurements in reconstructed images

G.2. IMAGE REGISTRATION

G.2.1. Introduction

We have investigated a surface-fitting image registration program for correlating SPECT and PET (ECT) images with MR. The registration is important for a number of reasons. First, the better resolution and anatomical delineation in the MR images may allow improved ROI analysis in the ECT images. In addition, the registration with MR images provides anatomic localization of ECT lesions. Also, the boundary from the MR images may used to improve the ECT reconstruction through Bayesian techniques. Finally, image registration may be used to correlate serial scans from the same modality. This allows better assessment of lesion change.

The general procedure for surface fitting was developed at the University of Chicago [Pelizzari et al 1989]. It consists of determining contours of the volume(s) of interest in several slices in each of the two multi-slice image sets to be matched and then determining the appropriate transformation (including translation, rotation, and scaling) to match the thus-defined surfaces. Once the appropriate transformation has been determined, one multi-slice set may then be re-sliced to obtain slices which match the anatomy of the other set. The registration may then aid in the visual evaluation of the images, or may aid in

reconstruction and/or quantitative analysis of the ECT images.

The high-resolution structural information made available through registered MR would be valuable for quantitative SPECT MoAb imaging since the objects of interest (both normal body uptake and tumor uptake) are often small relative to the system resolution. We are pursuing various means of determining surfaces for the brain and other body parts in the case where the lesion is hot relative to the surrounding tissue. Such means include using the reconstructed scatter window and using simultaneously acquired transmission images.

Our initial research has involved assessing the accuracy of this technique for registration of brain images, as well as improving the initial surface determination in the ECT images.

G.2.2. Improvement and Automation of the Surface Fitting Technique for Brain Image Registration

The quality of the fit performed by the surface fitting program depends on the ability to define the brain edges in the original images. The resolution contrast of the MR images (~1 mm) makes brain edge determination fairly straightforward by using a threshold which is some fraction of the brain matter pixel values and searching in from the lower intensity skull region until hitting this threshold.

The edges of the lower-resolution ECT images, however, are not so straightforward to detect, or, more precisely, determining an edge which corresponds to the MR edge is not so straightforward. This problem extends to any application of the surface fitting, including regions other than the brain. Using a simple threshold which is a fraction of the hottest pixels in the grey-matter regions is not suitable since the non-uniformity in the thickness of the cerebral cortex leads to different maximum values along different inward spokes, so that different thresholds would need to be applied.

We have found that using a first-derivative maximum leads to edges in ECT images which match the MR image edges well. In this process, differences between neighboring pixels values are calculated along all of the inward spoke leading to the center of the brain. On each inward spoke, the first pixel which is a local maximum in the difference value and whose value is above a predetermined noise threshold is called an edge point. Radial smoothing of the resulting contours is applied, and when these surfaces are fit to the corresponding MR surface for human registration studies, the scale factor required to best match the two surfaces generally deviates from 1.0 by less than 1% in each dimension.

G.2.3. SPECT Evaluation of Accuracy Using 3D Brain Phantom

The first test of the accuracy of the surface fitting procedure was done by registration of SPECT image sets to other SPECT sets [Turkington et al 1991b]. This has clinical relevance for comparing serial studies to look for tumor changes, etc. A three-dimensional brain phantom [Hoffman et al 1990] was filled with ^{99m}Tc solution and scanned at five different orientations in the SPECT scanner. Surfaces were defined for each of the individual sets and the surface fitting program was used to find the correct transformation. Markers which had been placed on the outside of the phantom were used to measure the accuracy of the surface-fit-determined transformation. Table 1 shows the errors as measured from the markers in various parameters when each of the five scans was compared to each of the others.

Table 1. Error in surface fit registration comparing different SPECT scans of brain phantom.

	rms error (mm)			mean error(mm)			angle error(deg.)		
scans	x	y	z	x	y	z	z	y	x
1 to 0	0.4	1.4	1.7	-0.1	0.8	0.5	-0.1	0.3	1.4
2 to 0	0.9	1.1	1.6	-0.0	0.8	1.1	-0.1	-0.9	0.7
3 to 0	1.6	0.8	2.6	0.4	0.0	1.1	0.7	-1.7	0.2
4 to 0	1.0	0.7	1.4	0.4	0.3	0.5	0.9	0.2	-0.2
2 to 1	2.7	2.1	3.7	1.0	1.2	1.9	-0.8	-2.4	1.3
3 to 1	3.1	1.7	4.4	1.4	0.9	0.9	-1.1	-2.9	1.6
4 to 1	2.3	1.2	3.4	1.2	0.1	0.5	2.1	-0.2	-1.2
3 to 2	1.0	0.9	1.9	0.6	0.4	0.3	-0.2	-0.9	0.9
4 to 2	2.0	2.6	1.1	0.4	-0.1	0.0	0.9	1.7	0.5
4 to 3	2.0	2.6	1.0	0.3	0.5	-0.2	0.8	1.7	0.2

G.2.4. SPECT, PET, and MRI Evaluation Using 3D Brain Phantom

The same phantom was also imaged in MR and PET to evaluate accuracy for registration of SPECT and PET to MR [Turkington et al 1992a]. Markers which were present in all scans were used to measure the accuracy of the surface fit for five different SPECT image sets and three different PET sets all registered to an MR set. The results are shown in Table 2.

Table 2. Errors in surface fit registration between ECT and MR images of brain phantom.

	rms error(mm)			mean error(mm)			angle error(deg.)		
scans	x	y	z	x	y	z	z	y	x
SPECT1 to MR	-0.1	-1.6	-1.2	1.4	1.9	2.1	-0.1	-0.9	0.9
SPECT2 to MR	-0.8	-1.1	-1.6	1.8	2.2	3.0	0.6	1.0	1.9
SPECT3 to MR	-1.3	-0.2	-2.2	2.1	3.2	4.2	-1.2	1.0	2.9
SPECT4 to MR	-0.4	-2.0	-1.0	1.4	2.4	1.4	0.8	-0.5	2.9
SPECT5 to MR	-0.2	-0.4	-0.5	1.4	1.6	1.4	0.5	0.6	1.1
PET1 to MR	-0.4	-1.4	-2.3	1.4	2.6	2.9	0.5	0.6	1.4
PET2 to MR	-0.2	-0.6	-2.2	1.5	3.3	2.8	-1.4	-0.1	1.7
PET3 to MR	0.1	-0.7	-3.0	1.1	2.9	3.6	0.3	0.4	2.3

G.2.5. Evaluation Using Human Volunteers

Finally, the technique was evaluated on five human volunteers in PET and MR imaging [Turkington et al 1992b]. These persons had markers attached to their forehead and temple regions. For PET, three multi-slice ^{15}O-labeled water studies were done, and three ^{18}F-labeled FDG studies were done. These were surface-fit to 2 mm slice thickness MR volume acquisitions and the markers showed registrations errors less than 2 mm.

G.2.6. Registration of Human Brain Tumor Using SPECT Scatter Data

A mode of cancer therapy for cystic brain tumors is being investigated at Duke in which radiolabeled MoAbs are injected into an Ommaya reservoir with a tube connecting it to the tumor. These reservoirs are placed surgically to provide a means of extracting fluid from the tumor to relieve pressure. In both cases thus far, the 81C6 antibody has been labeled with ^{131}I for therapy. Prior to the therapy, the patients have undergone transmission CT, MRI, PET-FDG, and SPECT HMPAO imaging. In addition, studies were done to ensure that the reservoir-tumor system was closed so that the injected therapeutic dose would not leave the tumor. First, ^{99m}Tc HSA was injected into the reservoir. SPECT and planar images were acquired twice over a one day period. Then, ^{123}I-labeled 81C6 antibody was injected into the reservoir followed by several scans over a two-day period.

It would be desirable to register these SPECT studies with the MR image sets to ensure that activity is all staying within the bounds of the tumor as well as to ensure that it diffuses throughout the tumor volume. Using markers on the patient would be difficult since these studies are done over a period of several days. Therefore, we are attempting to use a head surface as determined from scatter window data to match with a head surface as determined from the MR image sets. This will enable us to use the surface fitting registration technique which we have found to work well in other contexts of brain imaging.

This general technique would be valuable whenever hot lesion SPECT images of the brain are to be registered with MR or transmission CT images, in particular with antibody tumor imaging using either intratumoral injection or intravenous injection.

We have reconstructed images from the scatter projection data using FBP and ML-EM methods. One slice from each method is shown in Figure 2. For these images, the photopeak projections were smoothed, multiplied by 0.4, and subtracted from the scatter data to reduce the effect of the intense source activity in the scatter window images. The low number of projection counts causes characteristic backprojection streaking to dominate the edge. Since the probability of a point being a scatter location decreases with distance from the location of the activity, the intensity far from the lesion is much lower than the intensity near the lesion, so that the edge is much more clear near the tumor. We have found that an ML-EM reconstruction of the scatter data yields a better edge as shown in the figure. We have not yet developed any automatic means of determining these edges.

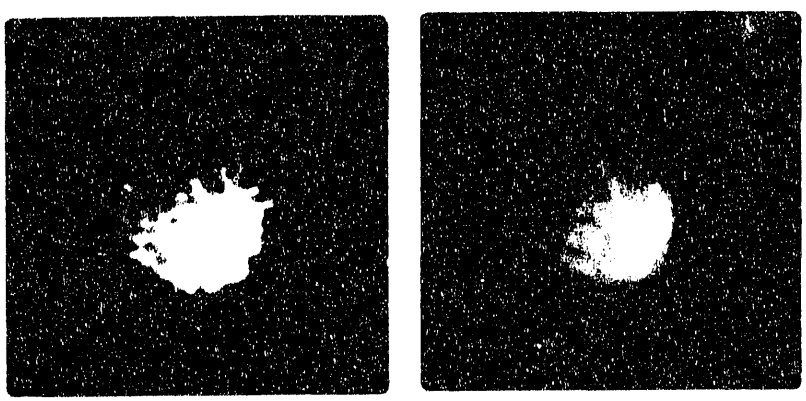

Figure 2. Reconstructed scatter data for hot lesion image. FBP is at left and ML-EM is at right.

An attempt to fit the surfaces determined from the SPECT scatter window with the surfaces from outer flesh in MR T1-weighted images has shown promise, although the SPECT surfaces are about 10% smaller. This could be in part because of the semi-automatic threshold method used to define the edge has not been optimized for these images. In addition, no rigorous attempt has yet been made to objectively determine contours in the reconstructed scatter images, nor to accommodate the inconsistent nature of the scatter data in reconstruction.

G.3. "SPECTER" SOFTWARE FOR QUANTITATIVE IMAGE ANALYSIS AND DISPLAY

A general-purpose program ("SPECTER") for analysis and display of multi-frame medical image sets has been written to run in the X window system. This program reads images from arbitrary file formats and contains many functions involving image display, profiles, and region-of-interest analysis. The program is used by several groups at Duke for displaying and analyzing SPECT, PET, and MR images. It is valuable in our networked Unix workstation environment since it allows images to be displayed across the computer network. The program handles display on existing Sun, Stardent, Silicon Graphics, and DEC workstations, as well as IBM and Macintosh personal computers.

G.4. SPECT MONTE CARLO PROGRAM

A decade ago, John Beck, a Ph.D. student working under Dr. Jaszczak's supervision, developed one of the first Monte Carlo programs to model a rotating-camera SPECT system [Beck et al 1982]. Using this early program as a basis, we have developed a new Monte Carlo program to simulate non-uniform objects for emission and transmission imaging systems [Wang et al 1992a, 1992b]. Although this research is funded primarily by our NIH grant (CA33541), it is briefly described here since it has been modified to provide simulated projection data for this DOE project, and its availability has facilitated our research efforts relating to SPECT MoAb imaging. The program can simulate projection data containing separate degrading effects such as attenuation, scatter, and collimation. Simulated projections with separate effects are useful for the development and evaluation of image reconstruction algorithms.

When evaluating and refining a specific algorithm, several different source geometries may be required. These source distributions may include either simple or complex geometries, including non-uniform attenuation and/or complex source shapes. Therefore, it is useful to have a flexible simulation program, and one that is capable of generating these projection data without excessive computational burden. To achieve this goal, we have developed a constructive solid geometry approach to model simple and complex source geometries [Wang et al 1992a, 1992b]. This approach can model both uniform and non-uniform attenuation. The solid geometry object model consists of two primary components: a set of object primitives and an inclusion tree. The object primitives include ellipsoids, elliptical cylinders, tapered elliptical cylinders, rectangular solids, and their halves, quarters, and eighths. The inclusion tree is a data structure to organize the inclusion relationships among the regions of an object. The shape of an object is expressed as a combination of object primitives based on set union, intersection, and difference. The primitives are then assigned material characteristics including density and energy-dependent photoelectric and Compton cross sections. Note that primitive overlaps are allowed for solid geometry models to create irregularly shaped objects. If primitive combinations are restricted to be without primitive overlapping, the solid geometry model is equivalent to the existing simple geometry model for simple objects. If an object is modeled by a union of rectangular solids with the same size, the solid geometry model is reduced to the existing voxel based model for highly complex objects.

Our Monte Carlo program with the implementation of the solid geometry object model has been validated. The validation was performed in three steps for the following media types.

Step 1. Non-uniform attenuation alone.

Step 2. Uniform attenuation and detected Compton scattering.

Step 3. Non-uniform attenuation and detected Compton scattering.

For Step 1, the Monte Carlo simulation of a thorax phantom was compared to a mathematical (non-Monte Carlo) simulation. The comparison was based on images reconstructed by a modified Chang technique [Chang 1978] for non-uniform attenuation correction. For Step 2, the scatter fraction of a point source in a water-filled cylinder was used to validate our scatter model for uniform scattering media. The difference between simulated and experimental results is on the order of 7%. For Step 3, a thorax phantom with a spherical source was used for validation. Normalized profiles across the center of the sphere projections for simulation and experiment were observed to have insignificant difference. These results validated the implementation of the solid geometry model in our Monte Carlo program. We are in the process of comparing our results with other Monte Carlo codes [Ljungberg et al 1990].

Our Monte Carlo program was originally developed on the Stardent GS1000 in our SPECT laboratory. The program has been ported to Cray YMP supercomputers at Florida State University for the simulation of highly complex objects requiring projections with high count density. Our use of the Cray Supercomputer is supported by the DOE, and access to this facility has been of great benefit to our research program.

H. Development of TCT and SPECT Acquisition Geometries

H.1. Upgrade of Triple-Camera SPECT System

A recently awarded University Research Instrumentation grant (DE-FG05-90ER75577) funded by the Department of Energy has enabled us to improve significantly the quantitative capability of our research SPECT system. We have obtained new ultra-high resolution collimators, an improved imaging table, upgraded scintillation crystals, photomultiplier tubes, electronics, and data processing software. The performance of the upgraded system has been evaluated quantitatively with several carefully implemented phantom studies. The results of these experiments have indicated that the overall performance of the upgrades is excellent.

H.2. Acquisition of Transmission CT Data with Triple-Camera SPECT System

Results from previous studies using ideal attenuation information [Gilland et al 1991a, Manglos et al 1987] have shown improved image quality with non-uniform attenuation compensation compared with uniform compensation. This motivated us to investigate methods to obtain attenuation maps using transmission computed tomography (TCT). To obtain these maps we have designed and built transmission data acquisition systems for the three-headed SPECT camera, providing the capability to reconstruct the 3D patient attenuation distribution.

Although the previous studies have shown that ideal attenuation information can improve image

quality and quantitative accuracy, it is still uncertain whether similar improvement may be obtained with real (experimentally acquired) attenuation information. Practical problems inherent in acquired transmission data, such as noise and resolution degradation, may limit the realized improvement [Greer et al 1987]. For this reason, we have chosen to design and construct a transmission data acquisition system for the three-headed SPECT system which is capable of acquiring and reconstructing attenuation information of the highest possible quality. This acquisition system uses a parallel beam transmission source. The question we wish to address in developing this hardware tool is the following: given high quality (but experimentally acquired) attenuation distribution information, does non-uniform attenuation compensation improve SPECT image quality?

Even if non-uniform attenuation compensation using acquired transmission data can be shown to improve SPECT image quality, the procedure cannot be used clinically if it does not meet the practical problems posed by patient imaging. Factors such as overall imaging time must be considered when scanning patients. In this regard, the parallel beam transmission source design suffers because the transmission and emission scans must be performed sequentially. In order to overcome this deficiency, we are currently designing a transmission data acquisition system capable of performing the emission scan using a fan beam transmission source. In this case the transmission source is located between two of the three heads so that only one head sees primary radiation from the transmission source.

H.2.1. Use of a Specially Designed Slab Transmission Source and Parallel-Hole Collimation: Initial Study

The transmission data acquisition system has evolved through three stages of refinement: flat slab source, curved slab source, and curved slab source with collimator. In all cases, the transmission source mounts between two of the three camera heads, allowing tomographic acquisition with the opposite head (Figure 3) . The two heads adjacent to the source are turned off. The flat slab source was 40 x 12 cm and 1 cm thick with a fillable volume of approximately 600 ml. This source geometry was used to evaluate non-uniform attenuation compensation with ^{111}In in phantom studies [Gilland et al 1991b]. Quantitative accuracy was improved when the transmission data collected with this source was used for non-uniform attenuation compensation. Due to the limited extent to which the adjacent camera heads retract, when this source is mounted on the SPECT system the maximum object radius was limited to approximately 15 cm.

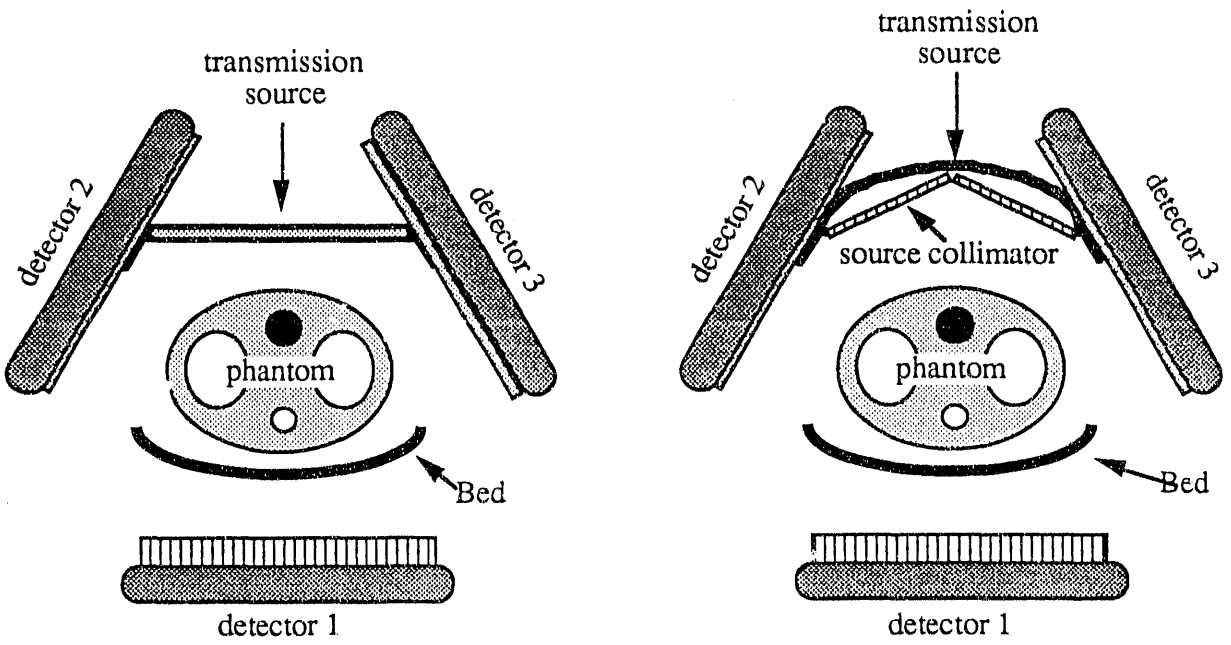

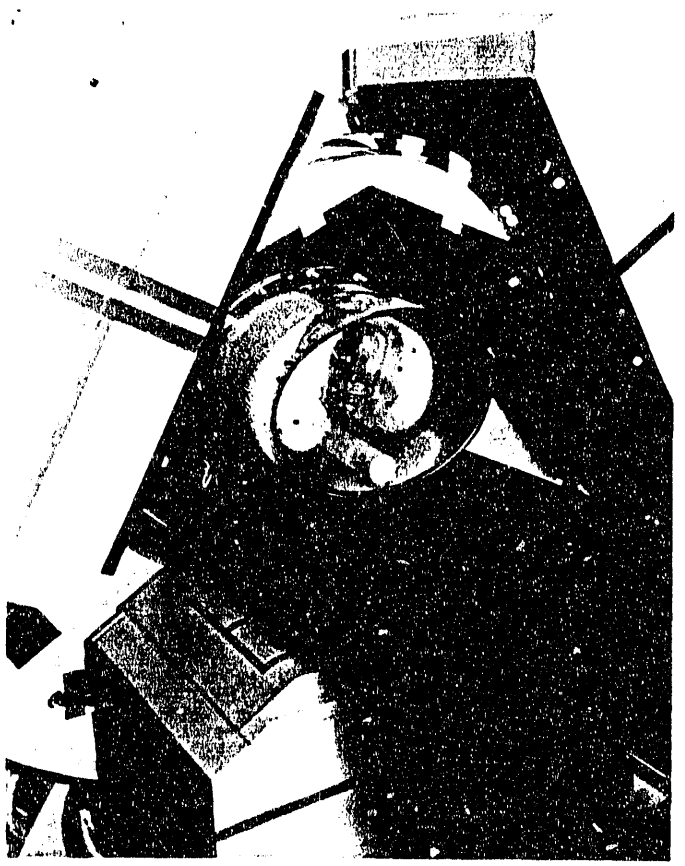

Figure 3. Transmission data acquisition using a flat transmission source (top left) and a curved transmission source with collimator (top right). Photograph of curved source is shown at bottom.

In order to accommodate human subjects a curved slab source was designed and constructed (Figure 3). This slab is approximately 50 x 12 cm and 1 cm thick with a 750 ml fillable volume. The curved source mounts to two camera heads similar to the flat source . This source was used for transmission data acquisition with both phantom and patient studies [Gilland et al 1991c].

In order to study the effects of transmission source collimation on the detection of scattered photons, the scatter fraction (ratio of scattered to unscattered photons detected) was measured with and without a standard low energy collimator placed between the curved slab source and an elliptical water-filled phantom. It was found that this collimator substantially reduced the scatter fraction in these images. Therefore, a customized collimator was designed and built for the curved transmission source in order to reduce scatter effects in the transmission acquisition. The collimator was constructed from two slant hole collimators which are mounted side-by-side and at an angle so that the holes of both collimators are parallel. The collimator assembly, then, can mount to the curved source and still have enough clearance to scan a large object. Scatter fractions were measured and the accuracy of transmission data reconstructions was evaluated with and without the transmission source collimator. The scatter fraction with a water-filled elliptical cylinder was reduced from 0.24 to 0.05 with the source collimator. Images reconstructed from tomographic transmission data of a chest phantom were more accurate with the collimator than without. The reconstructed attenuation coefficients with source collimator were accurate to within 5% in bone density and water density regions. Without the source collimator the reconstructed attenuation coefficient consistently underestimated the true value by approximately 12%.

H.2.2. Use of a Line Source and a Specially Designed Slit Source Collimator for Fan Beam TCT: Initial Study

The objective of this work was to determine the feasibility of using a line source/slit collimator (LS/SC) assembly coupled with an appropriate fan beam collimator with our triple-camera SPECT system to obtain transmission computed tomographic (TCT) data for brain and body attenuation maps. These maps may be useful for the following reasons: 1) to improve SPECT quantification by providing a means to obtain more accurate detection probabilities for our quantitative reconstruction algorithms; and 2) to provide anatomical data that would facilitate the registration of serial SPECT studies, or the registration of 3D SPECT image data sets with 3D image data sets from volumetric positron imaging (VPI), x-ray CT, and magnetic resonance imaging (MRI). The use of a line source and the triple camera SPECT system has the advantage that simultaneous fan beam transmission CT and emission SPECT data can be acquired simultaneously [for example, see Tung, et al 1992]. The use of a slit collimator in close proximity to the line source has the advantage that patient scatter and dose is reduced.

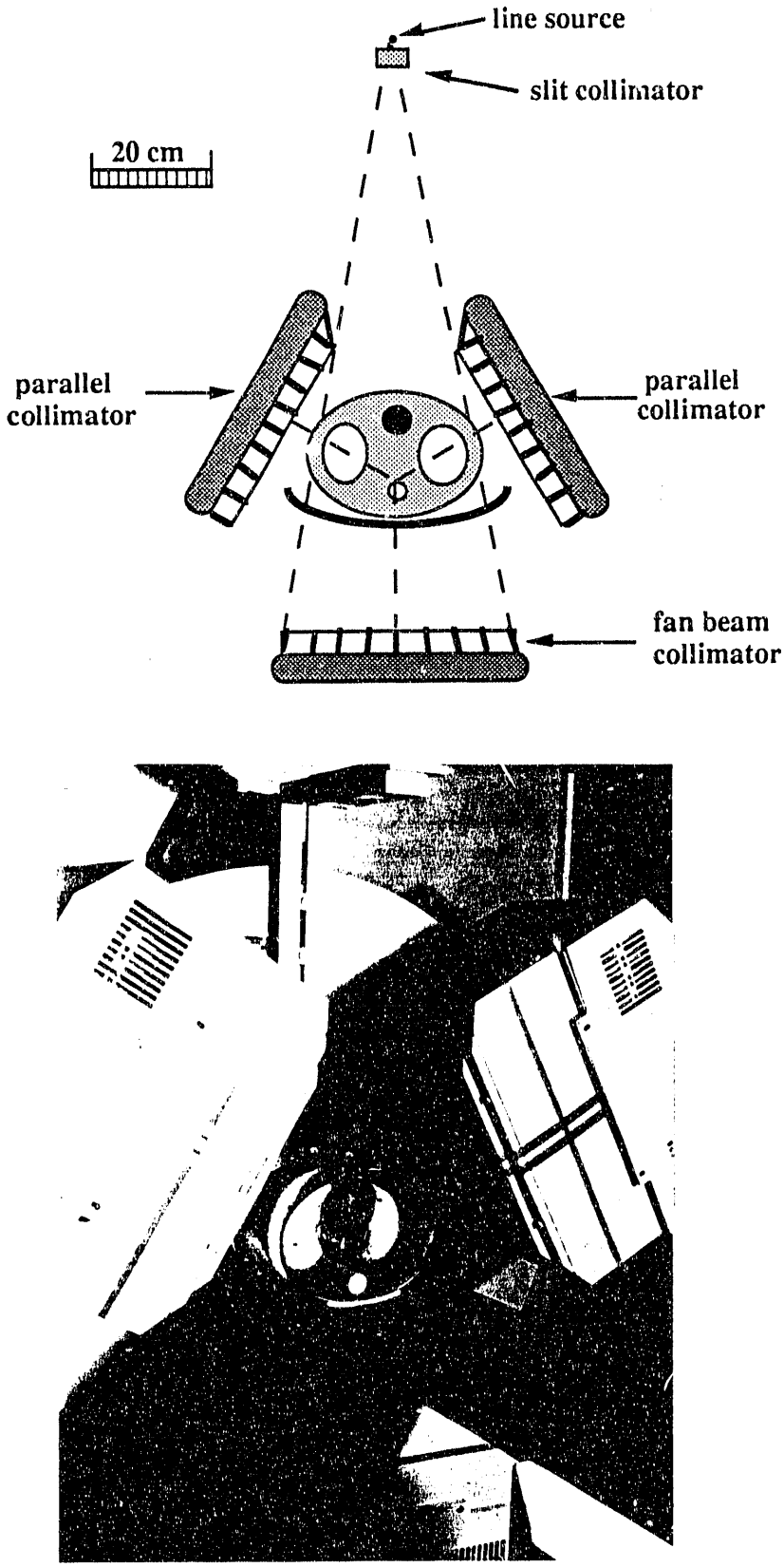

Figure 4. Sketch (top) and photograph (bottom) of line source/slit collimator for fan beam transmission CT. The bottom camera is used to acquire TCT data, while the other two cameras can be used to simultaneously acquire SPECT data.

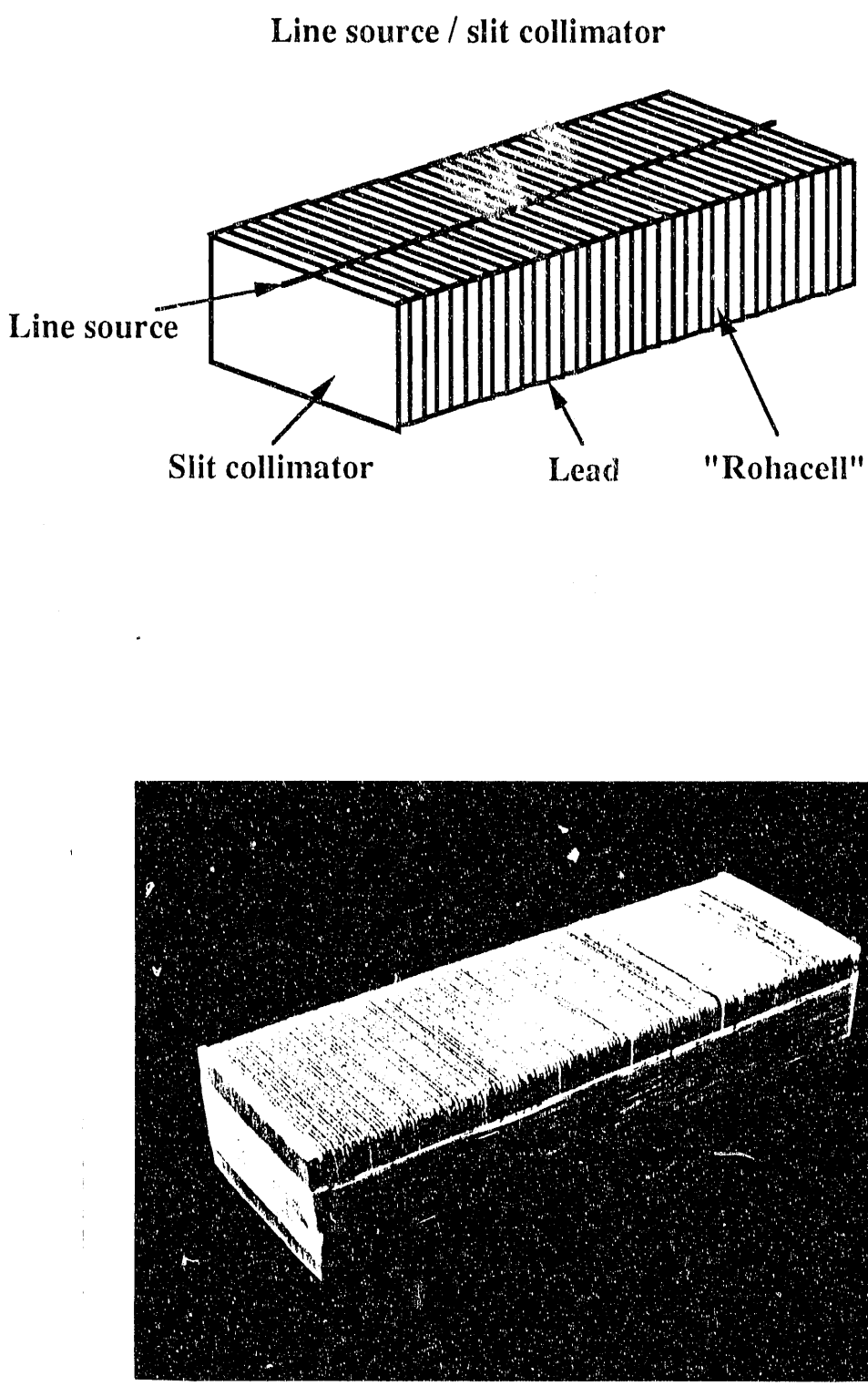

Figure 5. Sketch (top) of transmission line source/slit collimator assembly for fan beam transmission CT. Photograph (bottom) of slit collimator. The slit collimator consists of alternating layers of lead foil (0.25 mm) and Rohacell® (3.2 mm), which is a special "photon transparent" foam having highly uniform thickness.

The 20 cm long line source (1 mm capillary tube) was filled with approximately 5 mCi of Tc-99m solution and placed directly on top of the 20 cm long slit collimator. For this initial study, the complete LS/SC assembly was positioned directly above an uncollimated scintillation camera. The line source was placed parallel to the axis-of-rotation (AOR) and perpendicular to a line intersecting the center of one of the scintillation crystals of our triple-camera SPECT system. Thus, the LS/SC assembly was positioned between the other two cameras, since the three are equally spaced at 120 degree intervals. The use of an uncollimated scintillation camera allowed us to position the source at several different distances above the detector; hence, we were able to vary the "focal length" of the fan beam transmission source to determine the useful field-of-views (FOV) and the magnitude of truncation artifacts on the reconstructed TCT maps. Of course, a practical configuration would require that a fan beam collimator be placed on the TCT scintillation camera (see Figure 4), particularly if one wanted to simultaneously acquire SPECT data with the remaining two cameras of the triple-camera system. This would require, of course, that the line source contain a nuclide with a different photon emission energy than that of the nuclide being detected by the remaining two ECT-data collecting cameras. For, example, ^{133}Xe could be used as a transmission source when ^{123}I is used as the emission source. A sketch of the LS/SC assembly is shown in Figure 5.

Although the FOV generally increases as the LS/SC is positioned further from the camera, the maximum FOV possible is limited because of mechanical interference with the collimator housings for the other two SPECT cameras. For distances greater than approximately 110 cm the diverging fan of gamma rays impinges on the camera housings that are located at plus and minus 120 degrees from the TCT camera, particularly if these cameras are positioned close to the patient as they would be to acquire SPECT projection data. It was determined that a distance between 40 and 50 cm would be appropriate for imaging the patient's head. For body imaging, a distance of about 100 cm results in a useful FOV that is about 30 cm. This FOV is not quite adequate to obtain non-truncated TCT data for many subjects. To investigate the effectiveness of the LS/SC assembly, TCT scans were obtained of an elliptical cylinder (31 cm by 22 cm) containing anatomically shaped lung inserts for several different LS/SC locations above the TCT scintillation camera. For this study the lung inserts, containing styrofoam beads, were partially filled with water to obtain a density equal to approximately 0.4 the density of water. The surrounding volume of the elliptical cylindrical phantom and heart insert was filled completely with water. The attenuation maps obtained with the LS/SC positioned at the 100 cm demonstrated only minimal artifacts. The minor truncation artifacts were confined mainly to the edges of the elliptical cylinder along the major axis (Figure 6).

We, and other groups, [see for example Manglos et al 1991; Tung et al 1992] are currently investigating the significance of TCT truncation as it relates to SPECT attenuation compensation. It is reasonable to expect that minor truncation will not markedly degrade the SPECT reconstruction, and should provide improved quantification as compared, for example, with using an assumed constant attenuation coefficient. Our initial results indicate that TCT will be useful in improving SPECT quantification, and may be useful for providing additional anatomical information that could facilitate image registration for some SPECT studies.

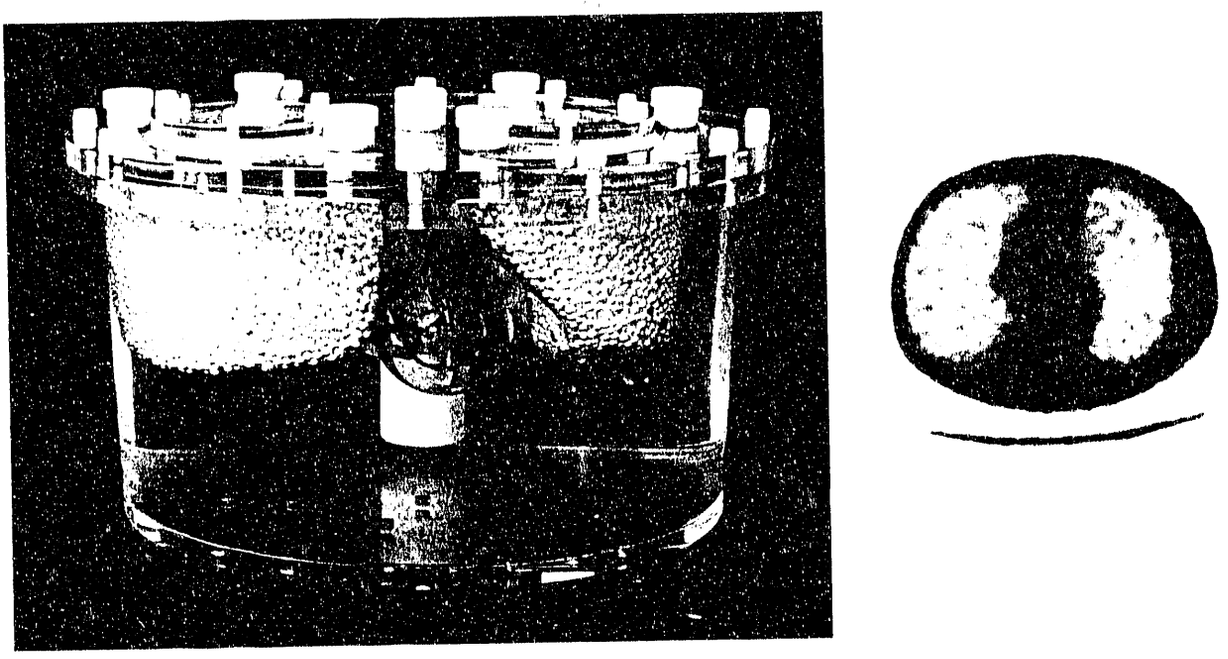

Figure 6. Photograph (left) of lung-heart phantom of a simulated thorax. Reconstructed fan beam TCT image (right) of experimentally acquired data of lung-heart phantom.

H.3. Pinhole Geometry SPECT for ^{131}I Imaging: Initial Study

There have been few studies directed towards the use of pinhole collimation with rotating-camera SPECT systems. Budinger [1980] described a hypothetical configuration consisting of several gamma cameras equipped with pinhole collimators. A few other investigators [for example, Rowe et al 1991; Palmer and Wollmer 1990; Olsson and Ahlgren 1990; Kearfott et al 1990; Rogers et al 1984] are investigating the use of pinhole or slit-type collimation as organ-specific or animal imaging devices.

Iodine-131 labeled MoAbs have a potential in radioimmunotherapy [Buchegger et al 1988] as well as in radioimmunodiagnosis [Chatal et al 1984 and Yeh et al 1991]. In applying SPECT quantification of ^{131}I for radiotherapy and radiodiagnosis, collimator septal penetration due to high energy (284(5%), 364(82%), 637(7%), and 723(2%) keV)) gamma rays is one of the most serious effects degrading image quality [Delaloye et al 1986; Yeh et al 1991]. Other image degrading effects include decreased crystal efficiency and inadequate sampling due to thick septa. Clinically, parallel beam, fan beam, and cone beam collimators are used widely for low and medium energy gamma rays (< 300 keV). For high energy gamma rays, either the septal thickness or the attenuation coefficient must be increased to reduce the septal penetration. To increase septal thickness, either the hole size or number of holes must be reduced. Reducing hole size and the number of holes results in less sensitivity and inadequate linear sampling. On the other hand, the most widely used material for collimators is lead. To increase the attenuation coefficient, materials such as tungsten, gold, and uranium [Francis et al 1962 and Hubbel 1969] can be used. The attenuation coefficients at 364 keV of lead, tungsten, gold, and uranium are 2.991, 4.105, 4.769, and 6.311, respectively. The cost of manufacturing collimators using these materials, however, is substantially higher than lead.

To circumvent the difficulties of imaging ^{131}I radionuclide distributions, we propose to investigate

SPECT data acquisition using pinhole collimators. The use of multi-pinhole apertures for SPECT are being investigated by other groups [for example, see Rowe et al 1991; Kearfott et al 1990]. A sketch of two pinhole collimator geometries is given in Figure 7. For pinhole collimators, the collimator penetration only occurs near the pinhole. To reduce penetration, the material near the pinhole can be enhanced by using tungsten, gold, or even uranium. The penetration for these materials is calculated for photons at 364 keV in Figure 8. Among the four materials of interest, uranium provides the best penetration reduction. The radioactivity of uranium, however, will create background and hence increase camera deadtime loss substantially. It is highly likely that this background activity will preclude the use of uranium. Based on this consideration, either tungsten or gold is a good choice for penetration reduction. Although the cost of tungsten and gold is much higher than lead, the cost of the collimator can be affordable if the collimator is made of lead with the small region near the pinhole made of tungsten or gold. In addition, the pinhole collimator requires only one hole instead of tens of thousands of holes as needed for parallel beam, fan beam, and cone beam collimators. The manufacturing cost can then be greatly reduced. Also, the manufacturing precision can be well controlled.

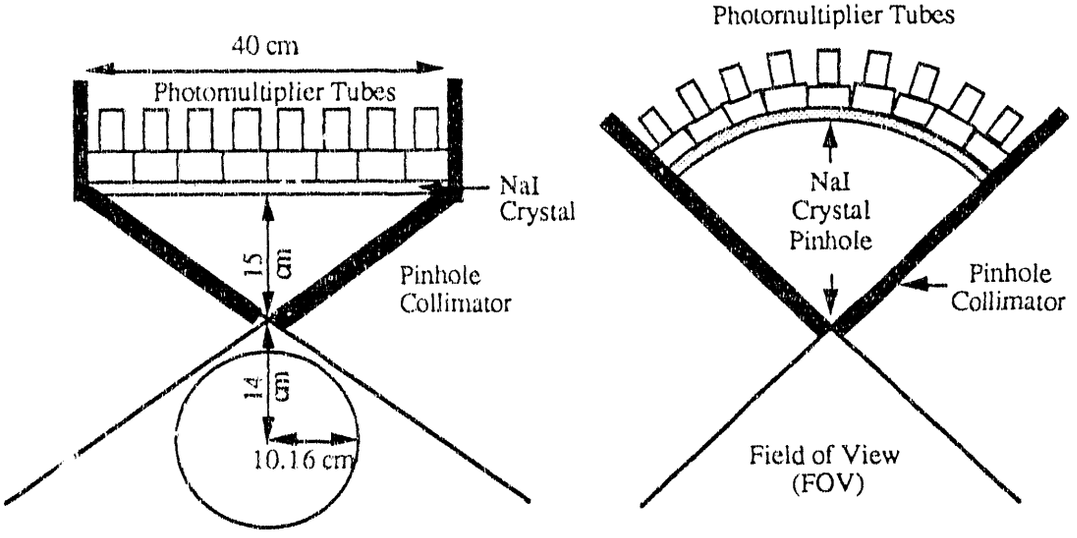

Figure 7. SPECT geometry for brain MoAb imaging using a flat (left) and a concave, spherical (right) NaI crystal.

Table 3 compares resolutions (Rpi) and sensitivities (Spi) of pin hole collimator at different distances (Dis) measured from the pin hole for different hole sizes (D). The material used for the pin hole collimator is gold and the penetration of γ-rays through gold is considered in the calculation. The effect of parallax error is not included. The focal length of the pin hole collimator is 15 cm and the diameter of the crystal is 40 cm. The field-of-view (FOV) is also listed in the table. For comparison, the resolutions (Rpa) and sensitivities (Spa) of a commercially available high energy parallel hole collimator are listed in the table.

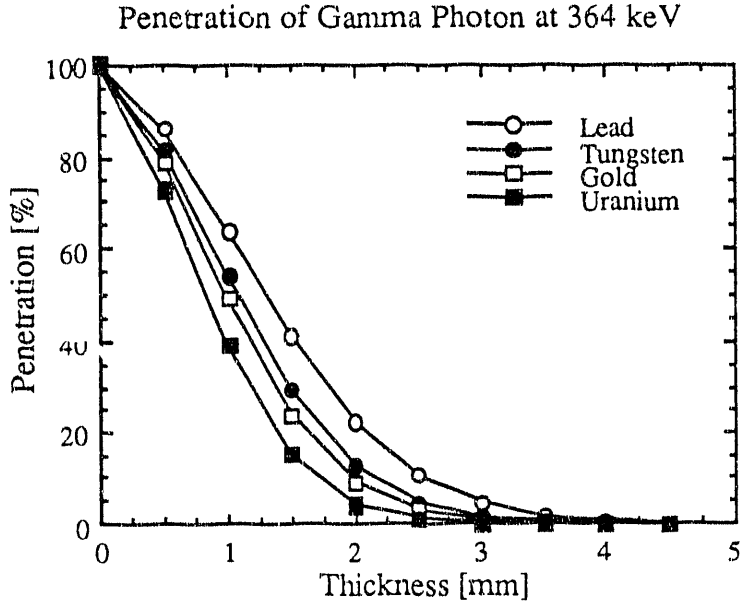

Figure 8. Penetration of 364 keV gamma rays through Pb, W, Au, and U.

Table 3. Comparisons of Resolution and Sensitivity

		Pin-hole Collimator (FL = 15.0 cm)						Parallel Collimator	
		D1 = 0.01 cm		D2 = 0.25 cm		D3 = 0.55 cm		Dpa = 0.45 cm	
Dis (cm)	FOV (cm)	Rpi1 (cm)	Spi1	Rpi2 (cm)	Spi2	Rpi3 (cm)	Spi3	Rpa (cm)	Spa
1.0	2.67	0.08	0.34E-3	0.47	0.12E-1	0.82	0.37E-1	0.61	0.17E-3
2.0	5.33	0.09	0.85E-4	0.50	0.31E-2	0.87	0.93E-2	0.68	0.17E-3
3.0	8.00	0.10	0.38E-4	0.53	0.14E-2	0.93	0.41E-2	0.76	0.17E-3
4.0	10.67	0.11	0.21E-4	0.56	0.76E-3	0.98	0.23E-2	0.83	0.17E-3
5.0	13.33	0.12	0.14E-4	0.59	0.49E-3	1.03	0.15E-2	0.91	0.17E-3
10.0	26.67	0.18	0.34E-5	0.75	0.12E-3	1.29	0.37E-3	1.28	0.17E-3
11.0	29.33	0.19	0.28E-5	0.78	0.10E-3	1.35	0.31E-3	1.36	0.17E-3
13.0	34.67	0.22	0.20E-5	0.84	0.72E-4	1.45	0.22E-3	1 51	0.17E-3
15.0	40.00	0.25	0.15E-5	0.91	0.54E-4	1.56	0.17E-3	1.66	0.17E-3
20.0	53.33	0.32	0.85E-6	1.07	0.31E-4	1.82	0.93E-4	2.05	0.17E-3
25.0	66.67	0.39	0.54E-6	1.23	0.20E-4	2.08	0.60E-4	2.43	0.17E-3

Material used for pin hole collimator is Gold, material used for parallel collimator is Lead
Crystal intrinsic resolution assumed is 0.20 cm, crystal diameter is 40 cm

D - diameter (hole size) of collimator
Dis - distance
FL - focal length
Rpa - resolution of commercially available high energy parallel hole collimator
Rpi - pinhole collimator resolution
Spa - sensitivity of commercially available high energy parallel hole collimator
Spi - pinhole collimator sensitivity

These comparisons indicate that besides the potential of minimizing the penetration and scatter of photons, pin hole collimators can obtain high resolution without sacrificing too much sensitivity. Another interesting feature revealed in the comparison is that ultra-high resolution (~1 mm) and moderate sensitivity can be obtained using a pin hole collimator if the object to be imaged is small. This feature indicates the potential use of pin hole collimator in imaging small animals. Of course, it would be necessary to design a system that either eliminates, minimizes, or compensates for parallax errors.

A preliminary study of imaging ^{131}I using pinhole collimators has been performed with Monte Carlo simulations. A Monte Carlo program has been developed in our SPECT laboratory to simulate anthropomorphic objects with non-uniform material characteristics including the photoelectric effect and Compton scattering [Wang et al 1992a, 1992b]. The program also includes parallel beam and cone beam collimation [Jaszczak et al 1992]. For the preliminary study, the program is modified to include pinhole collimation. A Jaszczak hot rod cylindrical phantom in Figure 9 is simulated by the modified Monte Carlo program. The attenuation and scatter in the phantom are not included for the simplicity of this first study. The simulated collimator has a 0.25 cm hole size and a 15 cm focal length.

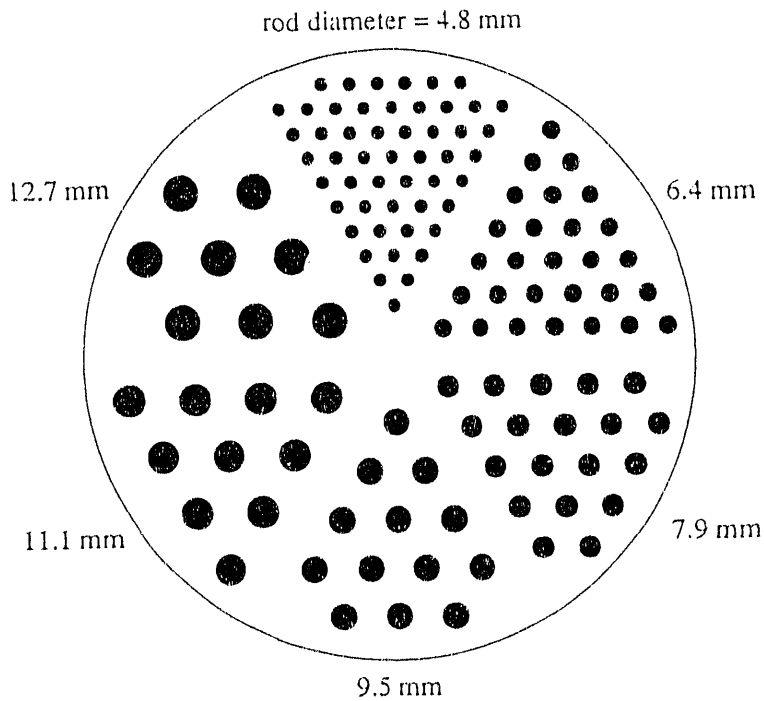

Figure 9. Sketch of "hot rod" phantom that was modeled using Monte Carlo simulations to obtain pinhole geometry SPECT projection data.

The simulated projection data consist of 180 equally spaced angular views over 360 degrees. Each projection set consists of a 256 by 256 array. The angular and linear sampling intervals are equal to 2.0 degrees and 1.6 mm, respectively.

A filtered backprojection (FBP) algorithm for pinhole geometries has been derived which incorporates the depth-dependent sensitivity into the back-projection process. Images of the hot-rod phantom are reconstructed using pinhole FBP. To reduce the computational burden, the projection data are reduced to an array having the dimensions of 128 by 128 by 180 angular views prior to reconstruction. The reconstructed image array consists of a cube having 128 by 128 by 128 elements. Figure 10 shows the transverse sectional image and profile of this phantom. The results of this preliminary study demonstrate the potential of pinhole collimators for ^{131}I SPECT imaging.

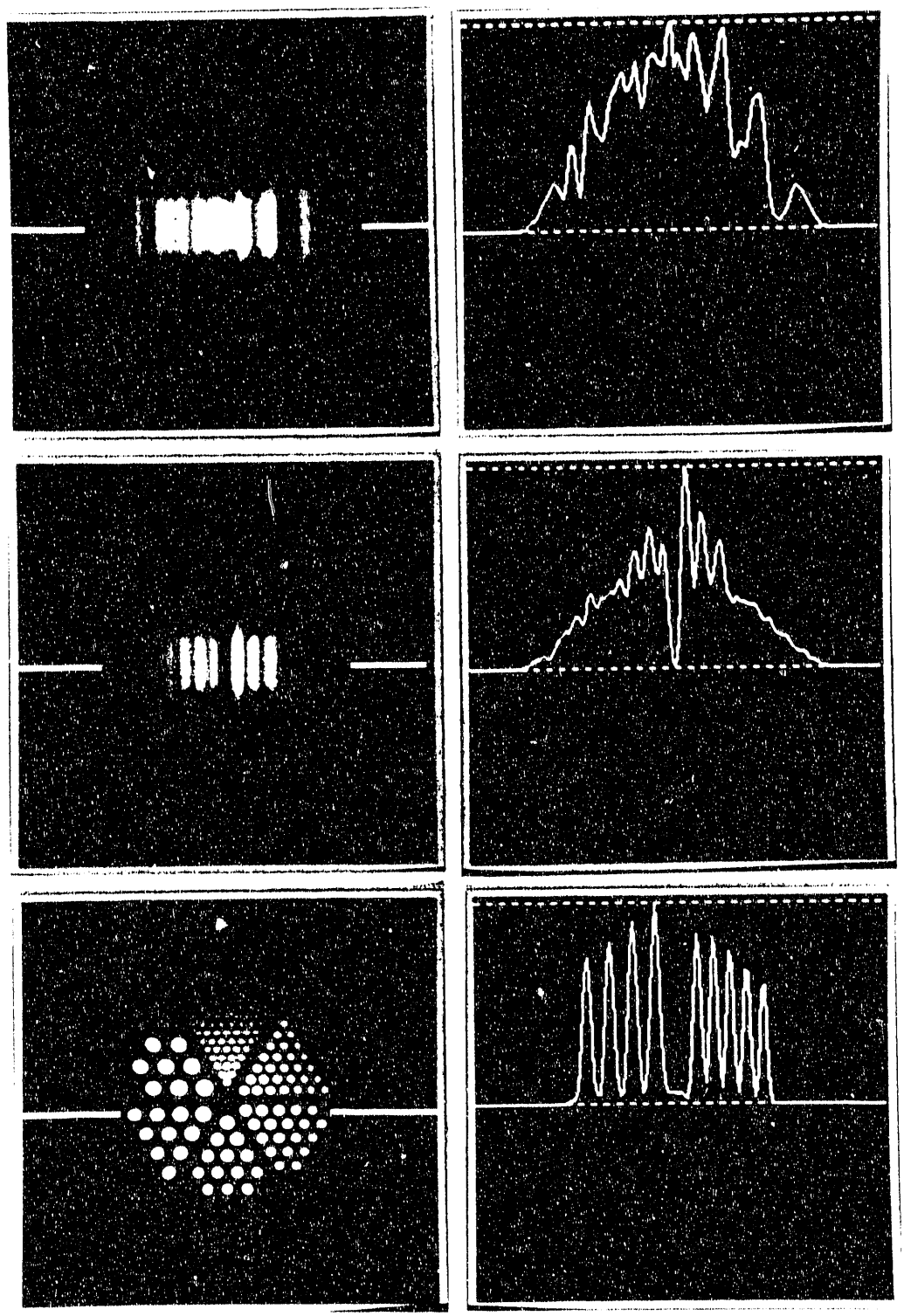

Figure 10. Sample pinhole geometry simulated projections (top 2 rows) and reconstructed transaxial image (bottom row) of hot rod phantom.

In practical SPECT imaging, attenuation and scattering in objects and collimator penetration are fundamental factors degrading image quality. To use pinhole collimators for high quality SPECT imaging, reconstruction algorithms considering such degrading factors are required. To study and develop ^{131}I SPECT imaging techniques using pinhole collimators, we will include the following works in our future research:

1. Incorporating attenuation, detected Compton scattering, and collimator penetration into our Monte Carlo program.
2. Developing three dimensional reconstruction algorithms for pinhole collimation with the consideration of attenuation, detected Compton scattering, and collimator penetration.
3. Evaluating the performance of SPECT imaging using pinhole collimators with simulations and experimentally acquired projection data.

Due to the high resolution capability, parallax error becomes more significant. Figure 11 shows the dependence of the parallax error on incidence angle for a NaI crystal with thicknesses of 5, 10, and 20 mm for photons at 364 keV. One way to reduce the parallax error is to reduce the crystal thickness. However, the decrease of crystal thickness can result in a loss of crystal efficiency. Figure 12 shows that a crystal with thickness greater than 5 mm can stop over 8% of the incident 364 keV photons for all incident angles. For the relatively high doses of ^{131}I that are used for therapy, this efficiency may be acceptable. For applications where the source intensity is limited, the following two approaches can be used to reduce parallax error. The first approach is to use a curved crystal [Lim et al 1980] for photon detection. With curved detectors, photon paths are almost perpendicular to the crystal surface. Hence the parallax error becomes insignificant, and thicker crystals can be used. The second approach is to incorporate the estimation of depth of interaction (DOI) into the interaction location calculation [Pouliot et al 1991]. Based on the DOI estimation, it may be possible to compensate for parallax errors. These aspects will be investigated in the future.

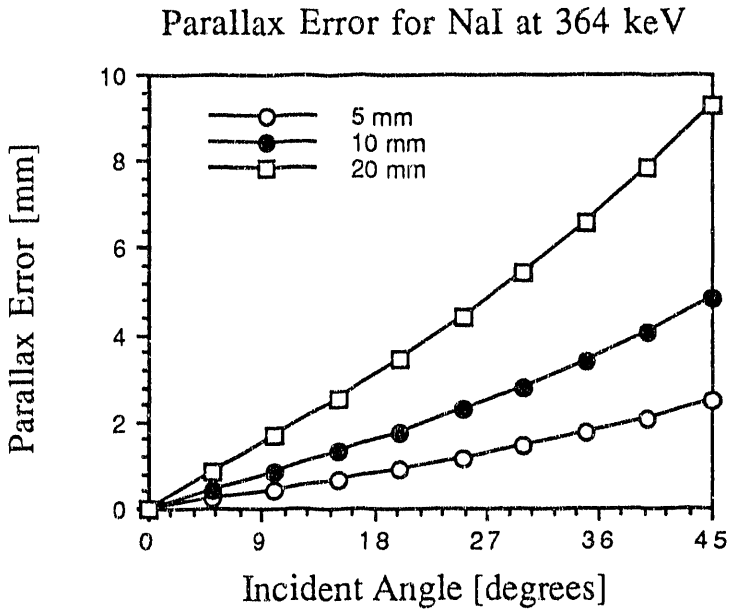

Figure 11. Parallax error as a function of thickness and angle of incidence.

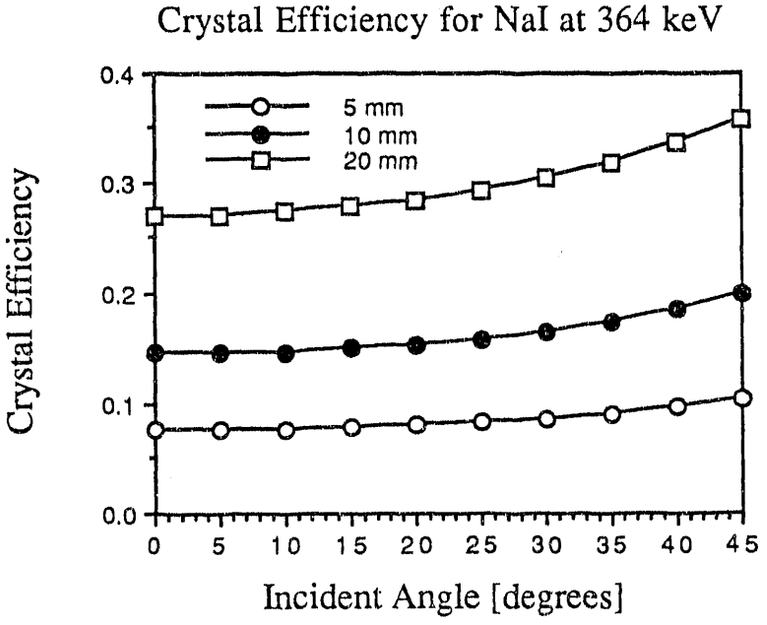

Figure 12. Efficiency of NaI crystal for 364 keV gamma rays.

H.4. Medium Energy Fan Beam Collimator Evaluation

Three custom-made medium-energy fan beam collimators were purchased for potential evaluation of measurement of *in vivo* antibody distributions in monkeys. The increased sensitivity of fan beam as compared with parallel beam collimators would result in improved imaging of the relatively low doses of ^{111}In typical in antibody studies.

As a preliminary step, the precision of the collimators' hole alignment was evaluated. The quality of the hole alignment was an issue, since inaccurately aligned holes would decrease the spatial resolution of the collimators, rendering them no better than lower-resolution parallel beam collimators with comparable sensitivity.

Extensive line source studies were performed on each of the three collimators. For the study, a capillary tube filled with ^{99m}Tc solution was placed above the collimator, parallel to the rotation axis (the y-direction). The tube was placed at various heights above the collimator and at various positions across the face of the collimator. Projection images were acquired for each tube position, and the linearity of line images was evaluated by fitting a straight line to the x-centroid at several locations along the length of the line. Figure 13 show a superposition of line source projection images with the line at different positions, all 15 cm above one of the collimators. Individual point deviations from the fit lines for all three collimators are shown in Table 4. The units are pixels (1.78 mm), which corresponds to 0.5 angular degrees since the source was 15 cm above the collimators. The deviations from linearity were converted to angulation errors using the height of the line source above the collimator, and the errors were found to be worse than the tolerance given in the specifications for the manufacturer. These collimators were returned to the manufacturer. We are currently investigating alternative collimator designs and suppliers.

Table 4. The rms deviation of fit lines from straight line in projection acquired with line source custom-made medium energy fan beam collimators.

	line source position (errors in pixels = 1.78 mm)											
rms errors	1	2	3	4	5	6	7	8	9	10	11	12
collimator 1	0.61	0.55	0.40	0.25	0.18	0.18	0.12	0.14	0.37	0.33	0.42	0.52
collimator 2	0.16	0.16	0.40	0.40	0.14	0.13	0.11	0.21	0.27	0.27	0.45	0.34
collimator 3	0.35	0.40	0.30	0.49	0.32	0.22	0.16	0.29	0.45	0.22	0.27	0.31

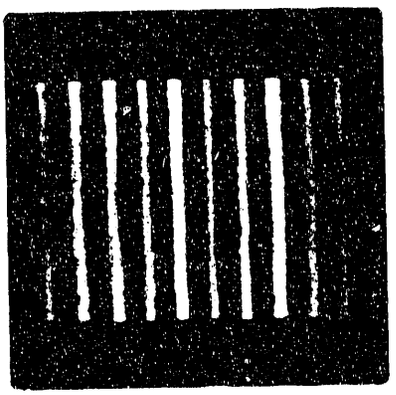

Figure 13. Composite line source image from one collimator.

I. Experimental Evaluations of SPECT Quantification: SPECT Quantification of Iodine-123

I.1. SPECT Quantification of Iodine-123: Phantom Studies

The major impediments to SPECT quantification with high purity ^{123}I are similar to the impediments with ^{99m}Tc: attenuation, scatter, finite spatial resolution, and image noise. Compensation for these effects with ^{99m}Tc data is often incorporated into the SPECT reconstruction algorithm. With ^{123}I data, however, these standard compensation techniques may be quantitatively inaccurate due to differences in energy spectra between the two radioisotopes. The objective of this work was to implement several SPECT reconstruction methods designed for ^{123}I data and to evaluate their performance in terms of quantitative accuracy, image artifacts and noise in phantom studies.

I.1.1. Methods

Four attenuation and scatter compensation schemes were incorporated into both the filtered backprojection/Chang (FBP) reconstruction algorithm [Chang 1978] and maximum likelihood-expectation maximization (ML-EM) algorithm [Shepp and Vardi 1982, Lange and Carson 1984] for a total of eight reconstruction methods under evaluation. The eight methods are sumarized in Table 5.

Table 5. Reconstruction Methods

Method name	Recon. algorithm	Attenuation map*	Scatter sub. (S) or Metz filter (M)
FBU	FBP	U/broad	
FBN	FBP	N/broad	
FBS	FBP	N/narrow	S
FBM	FBP	N/broad	M
MLU	ML-EM	U/broad	
MLN	ML-EM	N/broad	
MLS	ML-EM	N/narrow	S
MLM	ML-EM	N/broad	M

* U=Uniform attenuation map, N=Non-uniform attenuation map broad=broad beam attenuation coefficients, narrow=narrow beam attenuation coefficients

The methods were chosen in order to investigate the relative merits of FBP/Chang versus ML-EM reconstruction, uniform versus non-uniform attenuation compensation, and scatter compensation by broad beam attenuation map versus scatter subtraction by Metz filtering. The maps were similar in shape and differed, generally, only in their absolute magnitude.

The reconstruction methods were evaluated in a phantom study. The phantom consisted of a plastic cylinder with elliptical cross section containing low density wood "lungs", nylon "spine", and a hollow, plastic sphere. In the axial dimension, perpendicular to the elliptical cross section, the cylinder was 24 cm long. In cross section the lungs were 8.8 x 10 cm, and the spine was 2.5 x 2.5 cm (see Figure 16). The sphere was 3.5 cm in diameter. The inside of the cylinder, or background, and the inside of the sphere were filled with ^{123}I sodium iodide solution at concentrations of 1.3 and 6.7 μCi/ml, respectively. This study used ^{123}I produced by the (p,5n) reaction in order to reduce ^{124}I contamination and collimator septal penetration that is more prevalent with ^{123}I produced by the (p,2n) reaction.

The Chang compensation method [Chang 1978] was used in its single iteration form and generalized for non-uniform attenuation. The method used a previously described projector/backprojector [Gullberg et al 1985] to model non-uniform attenuation. The filter used for the FBP reconstructions was a ramp function with a Nyquist cut-off frequency (1.4 cycles/cm). The ML-EM algorithm used the attenuated projector/backprojector [Gullberg et al 1985]. The initial estimate was a uniform distribution, and the algorithm was stopped after 50 iterations. This iteration stopping point was selected after qualitatively examining reconstructions at 25, 50, and 100 iterations.

The scatter compensation methods investigated included scatter subtraction [Jaszczak et al 1984], Metz filtering [Metz 1969], and broad beam attenuation compensation. The scalar for the subtraction method was 0.4. The Metz filter used in this study was with the power parameter set to five. This parameter controls the shape of the filter, and five represents a reasonable compromise between image enhancement and noise suppression. The MTF function of the Metz filter incorporated an estimated scatter response function to provide scatter compensation. Broad beam attenuation compensation was accomplished by scaling the attenuation maps for reconstruction by 0.7.

The uniform and non-uniform attenuation maps used by all methods were computer simulated based on the known phantom dimensions and attenuation coefficients. The attenuation coefficients used for the non-uniform, narrow beam attenuation map were 0.17 cm^{-1} for nylon, 0.14 cm^{-1} for water, and 0.01 cm^{-1} for wood. The constant attenuation coefficient in the uniform attenuation map was computed as the average of the attenuation coefficients within the elliptical body in the non-uniform, broad beam attenuation map. All attenuation maps were filtered using a Hann filter with a cut-off frequency equal to the Nyquist.

Projection images were acquired using a three-headed SPECT system with medium energy collimators. The projections were acquired in a 128x128 matrix with a pixel size of 3.56 mm. There were 120 projection angles equally spaced over 360 degrees. The total scan time was 20 minutes. The photopeak energy window was 20% in width and centered at 159 keV, the primary emission energy of ^{123}I. Data from a lower energy window (100 to 140 keV) were also collected for scatter compensation.

The absolute quantitative accuracy of the eight methods was evaluated in the sphere, background, and lung regions. Count densities were measured in these regions of the reconstructed images using a five pixel ROI located in the center of the sphere and 20 pixel ROIs located in the center of each lung and in the background region between the lungs. From the count densities, the ^{123}I concentrations (μCi/ml) were computed based on the measured sensitivity of the SPECT system with medium energy collimators. The "true" concentration of each solution was based on planar camera measurements of 20 cc samples contained in a syringe and the measured camera sensitivity. As a measure of noise level, the relative noise magnitude, defined as the standard deviation of pixel intensities divided by the mean, was computed for each reconstruction method for the ROI located in the background region. In addition, profiles were drawn through the reconstructed images to further illustrate the noise level and quantitative accuracy of the reconstruction methods.

I.1.2. Results

The results of the quantitative analysis for the eight reconstruction methods are summarized in Table 6. The filtered backprojection method without compensation (FBP) has been included for reference using similar ROI measurements. The true activity concentrations are 6.7, 1.3, and 0 μCi/ml for the sphere, background, and lungs, respectively.

Table 6. Quantification and Noise Analysis

Recon. Method*	μCi/ml Sphere	Bckgrd	lungs	Relative Noise Magnitude**
FBP	1.90	0.35	.17	.317
FBU	4.65	0.96	.33	.219
FBN	5.12	1.22	.12	.165
FBS	6.34	1.14	0	.254
FBM	6.87	1.18	-.02	.150
MLU	4.65	0.88	.52	.175
MLN	5.25	1.18	.11	.144
MLS	6.61	1.17	.03	.207
MLM	7.14	1.26	-.06	.106

* see Table 5 for description of methods.

** standard deviation divided by the mean of pixel intensities within an ROI located in the background region.

Table 6 reveals a number of important characteristics of these reconstruction methods in terms of quantitative accuracy. First of all, there is dramatic improvement in both the filtered backprojection/Chang and ML-EM methods with non-uniform compared to uniform attenuation compensation. The count density in all three regions of the phantom is more accurate with non-uniform compensation. Figure 14 shows the reconstructions with profiles for the FBP/Chang (left) and ML-EM (right) methods with both uniform and non-uniform attenuation compensation.

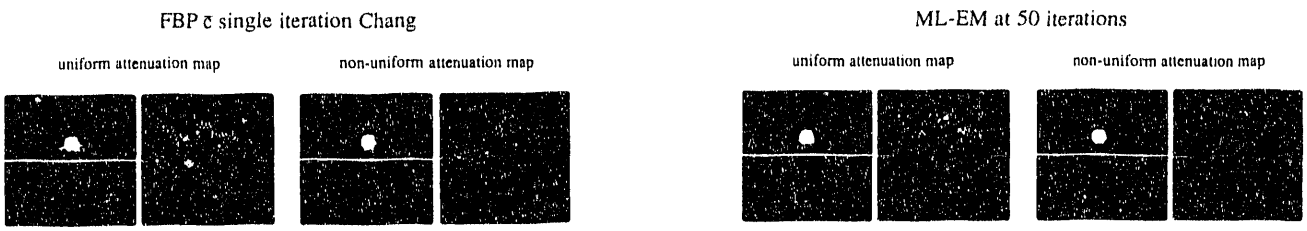

Figure 14. Filtered backprojection (left) and ML-EM (right) reconstructions with uniform and non-uniform attenuation compensation.

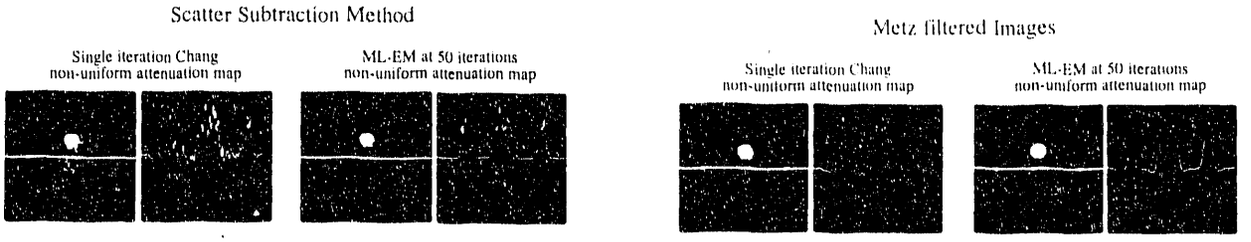

Figure 15. Scatter subtraction method (left) and Metz filter (right) applied to filtered backprojection/Chang and ML-EM reconstructions.

The scatter subtraction and Metz filter methods further improved the quantitative accuracy in these images. The count density in the lung region with the subtraction methods was closer to the true value of zero. Figure 15 shows reconstructions and profiles with FBP/Chang and ML-EM with both scatter subtraction (left) and Metz filtering (right). The figure illustrates the over-compensation in the lung regions and the smoother quality of the Metz filtered images as a result of the filter's suppression of high frequencies.

Table 6 also shows the relative noise magnitude measurements for each of the reconstruction methods including filtered backprojection. Within any individual compensation scheme, the ML-EM method had lower relative noise magnitude than FBP/Chang. This result is apparent in Figures 14 and 15 where the profiles through the FBP/Chang images show greater high frequency fluctuations relative to the ML-EM images. Within either the FBP/Chang or ML-EM method, the Metz filtered images had lowest noise followed by non-uniform and broad beam, uniform and broad beam, and finally scatter subtraction.

Figures 14 and 15 reveal artifacts of the reconstruction methods. For example, in both the FBP/Chang and ML-EM methods with uniform attenuation compensation a dark band connects the top of the lungs with the hot sphere and distorts the shape of both the sphere and lungs. With either FBP/Chang or ML-EM, non-uniform attenuation compensation removes this band. Also, in the FBP/Chang images high intensity streaks can be observed emanating from the hot sphere especially with the scatter subtraction images. This could possibly be due to the amplification of the high frequency edges of the sphere by the ramp filter followed by backprojection. In the ML-EM images these streaks are eliminated and the true shape of the sphere and lungs is reconstructed.

I.1.3. Conclusions

Of the compensation schemes evaluated in this study, the results suggest the most accurate reconstruction method for either the filtered backprojection/Chang algorithm or the maximum likelihood-maximum expectation (ML-EM) algorithm includes scatter compensation by either the subtraction technique or Metz filtering and non-uniform attenuation compensation . The results also suggest that the ML-EM algorithm can offer an advantage over FBP/Chang by providing lower image noise image noise for the same degree of quantitative accuracy. Non-uniform attenuation compensation offers significant improvement in quantitative accuracy and reduces image artifacts compared with uniform compensation.

I.2. SPECT QUANTIFICATION OF ^{123}I: *IN VIVO* STUDIES

I.2.1. Monkey Study

As a measure of quantitative accuracy of SPECT measurements of *in vivo* distributions of ^{123}I, a study was performed on a monkey (*Macaque fascicularis*) followed by measurements of extracted tissue samples.

The monkey was injected with the 81C6 MoAb labeled with 400 μCi of ^{123}I. Soon after injection, two SPECT scans were performed, each 30 minutes long. The three cameras were mounted with medium energy, low energy fan beam, and low energy ultra-high resolution collimators. Two energy windows were acquired, one 20% window centered on the 159 keV photopeak, and a 35% window adjacent to and below the photopeak. Acquisitions were 360 degrees. Following the scans, the monkey was sacrificed, and several of the organs were removed. Three small samples (approximately 1.0 g) each of the liver and spleen were extracted, weighed, and measured in a well counter.

Following the monkey scan, an ^{123}I source was scanned inside a bottle of approximately the same size as the monkey torso (~12 cm diameter) with the bottle empty and then full, for purposes of determining an appropriate attenuation correction. With a scatter subtraction factor of 0.5, an attenuation correction based on an empirically determined coefficient of 0.13/cm gave reconstructed images in water which best matched the images with no water. It should be noted that for these monkey studies, the scatter fraction is less than 10% because of the animal's small size.

Since significant redistribution of the activity was observed between the two monkey scans in the reconstructed images, only the second scan was used for comparison with the tissue samples. Images were reconstructed with FBP, with scatter subtraction (k=0.5), and Chang multiplicative attenuation correction based on uniform attenuation. The body contour was determined from the reconstructed scatter window projections. The liver and spleen were identified in the reconstructed images and total counts were measured by drawing ROI's which included all pixels within 10% of the peak counts for that organ. The background was sufficiently low that this loose ROI definition was permissible. The count total measured for each organ was normalized to the injected dose (as measured in a calibration scan before injection) and divided by the total organ weight as measured immediately after extraction.

In Table 7, the activity measured with SPECT is compared with the activity measured from the tissue samples. An assumption is made that the uptake was uniform throughout the liver and spleen.

Table. 7. Comparison of SPECT quantification with tissue activities.

percent injected dose/gram	liver	spleen
from scan	0.14	0.23
from tissue samples	0.126	0.191

J. Experimental Evaluations of SPECT Quantification: SPECT Quantification of Indium-111

J.1. SPECT Quantification of ^{111}In: Phantom Studies in Media with Constant Linear Attenuation

Quantification of the *in vivo* distribution of ^{111}In has clinical importance for such procedures as platelet and monoclonal antibody imaging [van Reenen et al 1982, Perkins and Primm 1985, Wessels et al 1985, Halpern et al 1988]. While the advantages of SPECT over planar imaging for quantifying ^{99m}Tc distribution have been recognized [Budinger and Gullberg 1974, Jaszczak et al 1977], SPECT has not been applied to a great extent for quantifying ^{111}In distribution [King et al 1986]. Studies aimed at quantifying with ^{111}In have relied mainly on conjugate view, planar techniques [Thomas et al 1977, Wu and Siegel 1984, van Rensburg et al 1988]. The emitted energy spectrum of ^{111}In poses unique problems for SPECT, especially with regard to attenuation and scatter compensation.

J.1.1. Methods

A phantom study was performed to evaluate SPECT ^{111}In quantification for hot objects with volumes from 12 ml to 1500 ml in a water-filled torso-shaped phantom with low-level background [Turkington et al 1991a]. The filtered backprojection was done using three different methods of correction for attenuation and scatter:

1. Summing projections from 173 and 247 keV photopeaks before reconstruction, subtracting scatter and narrow-beam Chang attenuation correction [Chang 1978].

2. Reconstructing 247 keV peak alone, subtracting scatter, and narrow-beam Chang attenuation correction [Chang 1978].

3. Reconstructing the 247 keV peak alone with broad-beam attenuation correction.

In all cases, the multiplicative Chang correction [Chang 1978] was done assuming constant attenuation, with the phantom edges defined through the reconstructed scatter window. Narrow-beam attenuation coefficients were based on book values, and the broad beam value was determined from another phantom study. The scatter subtraction factor was determined by imaging a cold sphere in a comparably-sized cylindrical phantom with surrounding ^{111}In activity.

Four separate acquisitions were performed, one longer one with higher count densities to study systematic effects, and three shorter ones from the three separate heads of the scanner. The shorter ones were performed to evaluate the effect of statistical fluctuations as well as the differences due to different uniformities and collimator irregularities. Total activity for each object was determined by drawing a loose ROI just big enough to include pixels at 10% of the peak value for that object in each slice containing part of the object, and the volume determination came from dividing the total counts for the object by the pixel values at the center of the object.

J.1.2. Results

The results from this experiment are shown in Table 8 for the higher count scans. Quantitative

accuracy of 7% or better was obtained for total object activity in all cases, and volume measurements were accurate to with 5% for the larger object, with increasing over-estimation for smaller objects since the method did not consider system resolution effects.

Table 8. SPECT Quantification of ^{111}In using three correction methods.

			total measured activity			measured volume		
obj	vol (ml)	activity	I	II	III	I	II	III
1	1435	2970	2771 (-7%)	2833 (-5%)	2808 (-5%)	1392 (-3%)	1374 (-4%)	1396 (-3%)
2	570	1600	1631 (2%)	1663 (4%)	1621 (1%)	576 (1%)	564 (-1%)	580 (2%)
3	95	433	410 (-5%)	418 (-4%)	413 (-5%)	99 (4%)	102 (7%)	103 (8%)
4	31.5	139	133 (-4%)	137 (-1%)	135 (-3%)	36 (14%)	38 (20%)	37 (17%)
5	12.5	57	57 (-1%)	58 (2%)	58 (1%)	20 (58%)	20 (58%)	19 (51%)

J.2. SPECT Quantification of ^{111}In: Phantom Studies in Media with Non-constant Linear Attenuation

The goal of this work was to investigate the capability of SPECT to accurately quantify ^{111}In distribution. The study compares several SPECT acquisition and reconstruction techniques in terms of their quantitative accuracy and image noise using experimental phantom data. These techniques include, first of all, non-uniform attenuation compensation using acquired gamma transmission data versus uniform attenuation compensation using an assumed attenuation coefficient and body contour. Secondly, the study compares independent reconstruction of the 172 keV and 247 keV emissions of ^{111}In versus combining the projection data from the two energy windows and reconstructing as one. Since attenuation and scatter characteristics are energy dependent, it is possible that improved reconstructions could result from handling the data from these two energies independently.

J.2.1. Experimental Phantom

The phantom used in this study was designed to simulate the non-uniform attenuation of the thorax. The phantom consisted of an elliptical, plastic cylinder containing non-porous, low density wood "lungs", a nylon "spine", and a hollow sphere. Three studies were performed using modifications of the non-uniform attenuating phantom. In the emission study the sphere was filled with ^{111}In solution at a concentration of 12 μCi/ml, and the cylinder was filled with a background solution of ^{111}In at a concentration of 2.5 μCi/ml. The lungs do not absorb activity. For the transmission study the sphere and cylinder were filled with non-radioactive water.

J.2.2. Data Acquisition

Data were acquired using a three-headed SPECT system. For both the transmission and emission acquisitions, 128x128 projection images were obtained at 120 equally spaced angles over 360 degrees with a scan time of 20 minutes. For the transmission study, ^{99m}Tc was the transmission source. The source holder consisted of an uncollimated flat plastic container mounted between two cameras of the three-headed system allowing a single head to acquire data (see Figure 3). Approximately 75 mCi of ^{99m}Tc in 600 ml of water filled the transmission source holder. The low energy, high resolution collimator was used, and the energy window was 126 to 154 keV (a 20% energy window centered at 140 keV).

Following the transmission study, the sphere and cylinder were filled with the appropriate concentration of ^{111}In , and the phantom was repositioned for the emission acquisition. Medium energy collimators were used. The emission data were acquired in four non-overlapping energy windows. Two were centered on the primary emission energies of ^{111}In (172 and 247 keV) and were 20% in width. The other two energy windows, one positioned below each photopeak window, provided an estimate of the scatter component in the above photopeak window for purposes of scatter compensation. The scatter window for the 172 keV emissions was 108 to 152 keV. The scatter window for the 247 keV emissions was 190 to 220 keV.

J.2.3. Image Reconstruction

The transmission data were reconstructed using the filtered backprojection method with a ramp filter with cut-off frequency equal to the Nyquist frequency. Before reconstruction the data were normalized to the incident intensity of the transmission source and logarithmically transformed. Negative values in the reconstructed image were set to zero, and a thresholding technique was used to zero pixels outside of the phantom boundary. In order to provide a higher count level attenuation map, four consecutive slices (slice width equaled 0.356 cm) of the transmission data were reconstructed and summed. Figure 16 shows an example of reconstructed transmission data at four slice (left) and single slice (right) thickness. All reconstructed images in this study were 128x128.

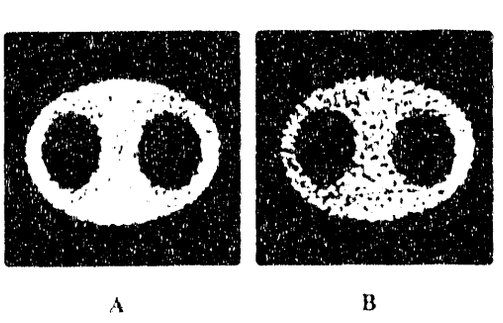

Figure 16. Reconstructed transmission data at four slice (left) and single slice (right) thickness.

Emission data were reconstructed with attenuation compensation using the "one-iteration" Chang method modified to provide the capability for non-uniform attenuation compensation. The attenuation map required by the Chang method for the non-uniform attenuation compensation was the four slice width transmission reconstruction (Figure 16, left). For the uniform compensation the attenuation map was a constant coefficient within the phantom boundary. The boundary was determined from the known position and dimensions of the phantom. The calculation of attenuation factors and the reprojection operation of the Chang method were performed using a ray tracing algorithm [Gullberg et al 1985].

The SPECT reconstructions of the emission study were performed using data from the 172 keV energy window only, the 247 keV window only, and the combined energy windows. The non-uniform attenuation map was scaled based on the energy window used in the reconstruction. Despite the fact that the total attenuation, considering both emission energies, scales non-linearly with the attenuation coefficients at the individual energies, this average coefficient was found experimentally to be within 3% of the measured attenuation coefficient of water to the ^{111}In emissions. This measurement was performed at 4.0 cm and 9.0 cm thickness of water.

For uniform compensation the constant attenuation coefficient used was the narrow beam value for the particular photon energy being reconstructed, or in the case of the reconstruction of the combined projections, the attenuation coefficient was the average of the 172 keV and 247 keV values.

Scatter subtraction was performed on the projection data before reconstruction . The scatter subtraction scalar k [Jaszczak 1984] was determined experimentally for the 172 keV, 247 keV, and combined data based on the line source measurements. For 172 keV, 247 keV, and combined data, k equaled 0.4, 0.6, and 0.4, respectively. Negative values in the subtracted projection data were set equal to zero.

J.2.4. Image Analysis

The quantitative accuracy of the reconstructed images was evaluated in the background, sphere, and lung regions. In the sphere and background regions the measured intensity, representing a count rate/unit volume, was compared to the count rate in a planar image of a 3 ml sample of the particular ^{111}In solution. The planar images provided a measure of the true count rate/unit volume for each solution in the absence of scatter, attenuation, and detector response effects. Quantitative accuracy in the sphere and background regions is reported in terms of percent error considering the planar count rate as the true count rate. Since the true activity concentration in the lung regions was zero, the absolute measured activity concentration in this region is reported.

As a measure of image noise, the relative noise magnitude, defined as the standard deviation of pixel intensities divided by the mean, is reported for a region-of-interest contained within the background region.

J.2.5. Results

Table 9 shows the results of the quantification and noise analysis for the eight reconstruction methods tested. The true concentrations are 12.0, 2.5, and 0 μCi/ml for the sphere, background, and lungs, respectively. With the exception of the sphere region for 247 keV data only/uniform attenuation compensation, all eight methods had an error of 16% or less. The methods which used both emission windows had substantially lower relative noise magnitude than the single emission energy images. In both

the uniform and non-uniform cases, the combined projections had slightly lower noise magnitude than the summed reconstructions. The count level in the lung regions is much closer to the true value of zero with non-uniform attenuation compensation than with uniform compensation.

Table 9. Quantification and Noise Analysis

		μCi/ml			Rel. Noise
		Sphere	Bckgrd	lungs	Mag.
true conc.		12.0	2.5	0.	
Unif. atten. recon.	172 only	12.0	2.3	.975	1.09
	247 only	14.5	2.3	1.26	.958
	172+247	13.0	2.2	1.09	.739
	com. prj.	13.1	2.3	1.17	.680
Non-unif. atten. recon.	172 only	10.1	2.3	.0024	.770
	247 only	12.4	2.4	.193	.757
	172+247	11.0	2.3	.306	.553
	com. prj.	11.1	2.4	.109	.526

Figure 17 shows the uniform (left) and non-uniform (right) attenuation compensated reconstructions for the 172 keV energy window data only, the 247 keV data only, the sum of these two reconstructions, and the reconstruction of the combined 172 keV and 247 keV projection data. The reconstructions which used both the 172 and 247 keV energy windows are qualitatively superior to the either of the single emission energy images in terms of image noise and artifacts. Differences between the summed reconstructions and the reconstruction of the combined projections are not readily apparent, even though the attenuation compensations were different for the two methods.

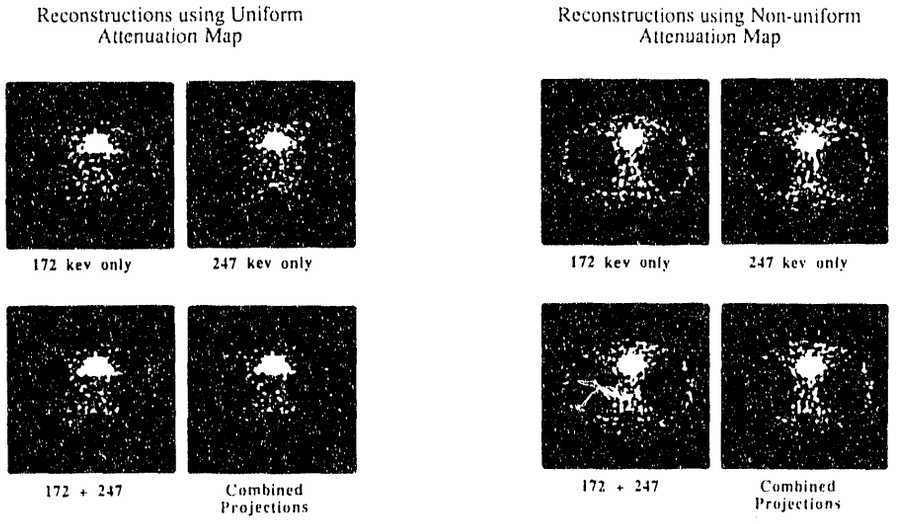

Figure 17. Uniform (left) and non-uniform (right) attenuation compensated reconstructions.

J.2.6. Conclusions

The results from this study suggest there is substantial improvement in terms of quantitative accuracy and image noise when both primary emission energies of ^{111}In are used. However, there does not appear to be any improvement in terms of either quantitative accuracy or image noise when the data from the individual energies are reconstructed independently compared with summing the projection data and then reconstructing. Since the latter method requires less data storage and processing time, this method is preferred. Non-uniform attenuation compensation using acquired transmission data greatly improved image quality and quantitative accuracy compared with uniform attenuation compensation.

K. Experimental Evaluation of SPECT Quantification: SPECT Quantification of Astatine-211

Astatine, which is a chemical analogue to iodine, has an isotope ^{211}At which emits 5.8 MeV alpha particles and is therefore potentially useful for therapy. In addition to higher energy gamma rays emitted at low intensity levels, 80 and 90 keV x-rays are emitted by ^{211}At, giving it potential for SPECT imaging as well as conventional nuclear medicine imaging. This allows the imaging of therapeutic doses, as well as allowing *in vivo* studies to compare the relative localization of ^{211}At-labeled antibodies to ^{123}I-labeled antibodies.

K.1. Methods

Preliminary investigation of the utility of ^{211}At for nuclear medicine imaging was performed. Three different collimators were used: a medium-energy collimator (MEDE) effective for photons up to 300 keV, a low-energy high-resolution collimator (LEHR), and a low-energy super-high resolution

collimator (LESR), all parallel hole. Pulse height spectra for the three collimators with an ^{211}At point source in air are shown in Figure 18. The dominant 80 keV photopeak is clear in all cases, as well as the effect of the lower-fraction 90 keV peak. The effect of the higher-energy photon emissions, as seen in the upper tail in all collimators, is least in the medium energy collimator, as expected.

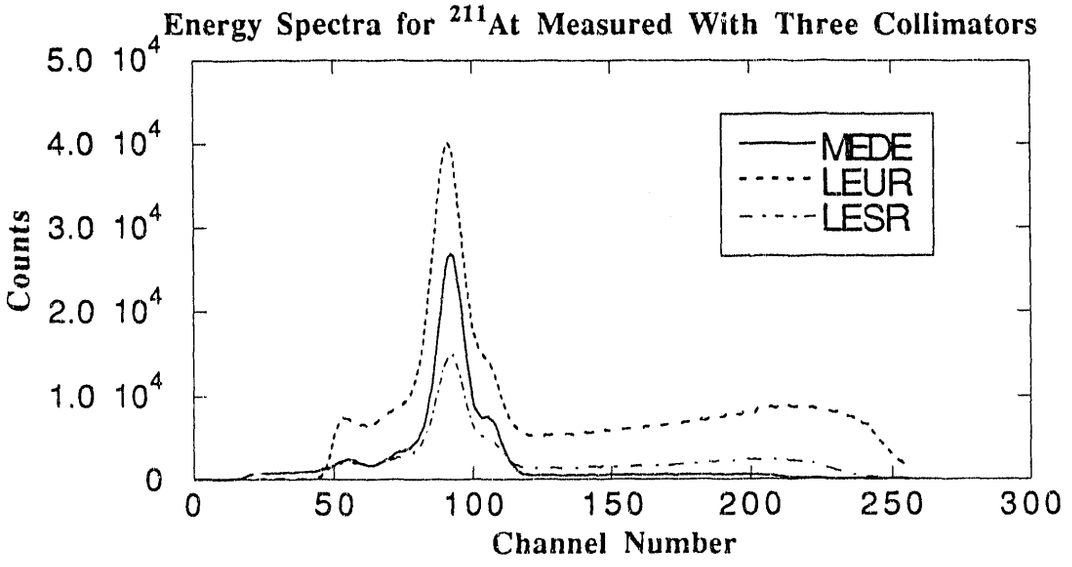

Figure 18. Energy spectra for ^{211}At with three collimators.

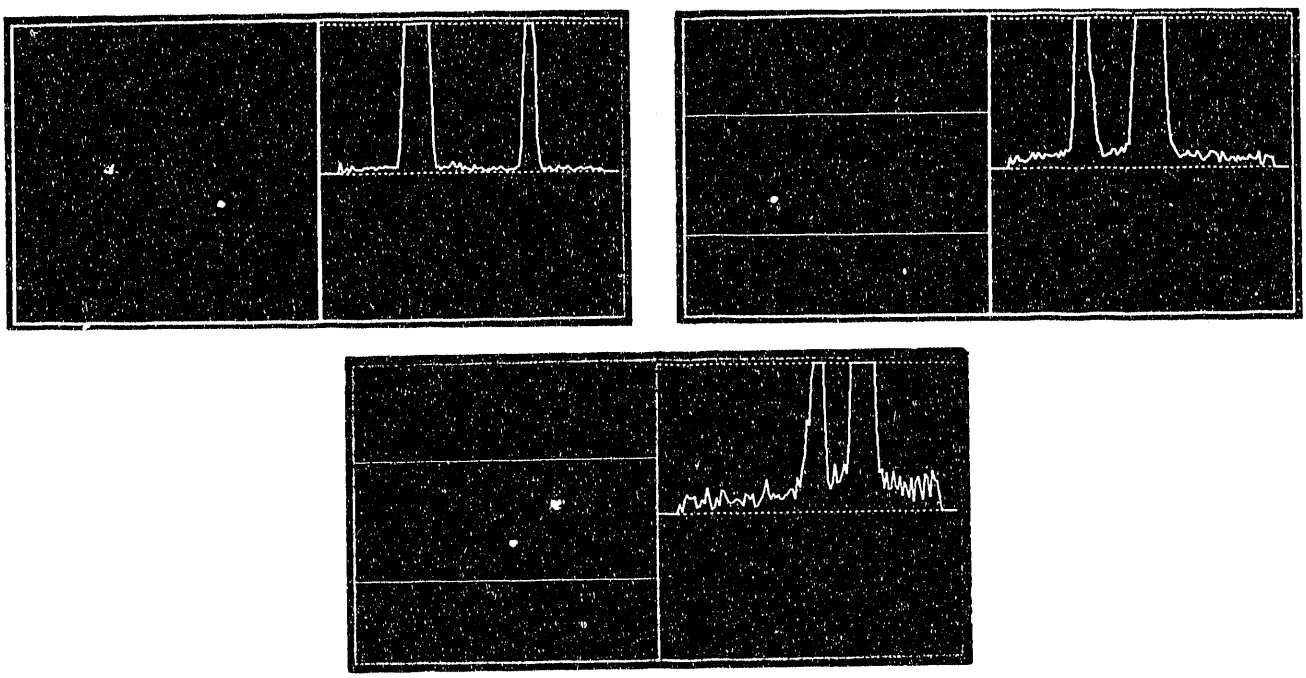

Figure 19. Projection images (different angles are shown) of ^{211}At point source and 30 ml sphere for MEDE (above left), LEUR (above right), and LESR (lower). Only the lowest 20% of profiles is shown.

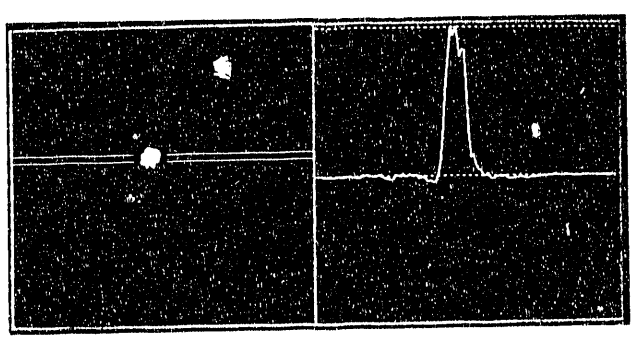

Figure 20. Reconstructed central slice and profile of 30 ml sphere in water with 200 μCi ^{211}At.

Projection images for a point source and a 30 ml sphere, each containing ^{211}At, are shown for the three collimators in Figure 19. Penetration is least for the MEDE, as would be expected, and is greatest for the LESR (relative to the collimated signal).

SPECT acquisitions were performed of the sources in air, and a SPECT scan was also performed of the sphere in a water-filled cylindrical phantom. The MEDE data were reconstructed and one slice through the middle of the sphere is shown in the Figure 20.

The possibility of quantitative SPECT imaging with ^{211}At was investigated by measuring the in-air counts from the sphere with the counts in water after scatter and attenuation correction. The Jaszczak scatter subtraction [Jaszczak et al 1984] method was employed, using a 30% window below and adjacent to the 20% window centered on the 80 keV photopeak. The subtraction constant was determined by comparing profiles of the sphere in projection images from the scatter window with those from the photopeak window, and determining a constant for multiplication of the scatter profile such that the tails matched the photopeak tails. This constant was determined to be 0.9. The multiplicative Chang attenuation correction method was used, with the edge of the cylinder determined from the the reconstructed scatter window projections. A narrow-beam attenuation coefficient of 0.18/cm was used. Total activity was measured by adding all counts in all slices containing the sphere, including all pixels within 3.6 mm of the center of the 2.0 mm radius sphere.

K.2. RESULTS

For the sphere in air, a value of 566 counts/sec was obtained, and for the sphere in water, 795 counts/sec, after correction for decay. The discrepancy is likely due to improper attenuation correction based on the assumption that only 80 keV photons were present. The higher energy photons would attenuate much less, and therefore less attenuation compensation would be necessary.

L. GLOSSARY

BME	Biomedical Engineering
DOI	Depth of interaction
FB or FBP	Filtered backprojection
FDG	Fluorodeoxyglucose
FOV	Field of view
FWHM	Full-width-at-half-maximum
GMI	Generalized matrix inversion
ISDS	Institute of Statistics and Decision Sciences (Duke University, Durham, N.C.)
LS/SC	Line source/slit collimator
μ	Linear attenuation coefficient
MC	Monte Carlo
ML-EM	Maximum likelihood-expectation maximization
MoAb	Monoclonal antibody
MR or MRI	Nuclear magnetic resonance (imaging)
MTF	Modulation Transfer Function
PET	Positron emission computed tomography
RID	Radioimmunodiagnosis
RIT	Radioimmunotherapy
rms	Root mean square
ROC	Receiver operator characteristics
SNR	Signal-to-roise-ratio
SPECT	Single photon emission computed tomography
SVF	Spatially variant focusing
TCT	Transmission computed tomography
VPI	Volumetric positron imaging

M. LITERATURE CITED

Beck JW, Jaszczak RJ,Coleman RE: Analysis of SPECT including scatter and attenuation using sophisticated Monte Carlo modeling methods. *IEEE Trans Nucl Sci* NS-29:506-511, 1982.

Buchegger F, Pelegrin A,Delaloye B: Iodine-131 labeled MAb fragments are more efficient and less toxic than intact anti-CEA antibodies. *J Nucl Med* 31:1035-1044, 1988.

Budinger TF: Physical attributes of single-photon tomography. *J Nucl Med* 21:579-592, 1980.

Budinger TF, Gullberg GT: Three-dimensional reconstruction in nuclear medicine emission imaging. *IEEE Trans Nucl Sci* NS-21:2-20, 1974.

Chang LT: Attenuation correction and incomplete projection in single photon emission computed toography. *IEEE Trans Nucl Sci* NS-26:2780-2789, 1978.

Chatal JF, Saccavini JC,Fumoleau P,Douillard JY: Immunoscintigraphy of colon carcinoma. *J Nucl Med* 25:307-314, 1984.

DeLaloye B, Bischof-Delaloye A,Buchegger F,von Fliedner V,Grob JP,Volant JC,Pettavel J. Mach: Detection of colorectal carcinoma by emission-computerized tomography. *J Clin Invest* 77:301-311, 1986.

Francis JE, Harris CC,Bell PR: A focusing collimator for research in scanning. *J Nucl Med* 3:10-17, 1962.

Gilland DR, Jaszczak RJ,Greer KL,Coleman RE: Quantitative SPECT reconstruction of Iodine-123 data. *J Nucl Med* 32:527-533, 1991a.

Gilland DR, Jaszczak RJ,Turkington TG,Greer KL,Coleman RE: Quantitative SPECT imaging with Indium-111. *IEEE Trans Nucl Sci* 38:761-766, 1991b.

Gilland DR, Jaszczak RJ,Coleman RE: Effects of non-uniform attenuation compensation in SPECT using acquired transmission data. *J Nucl Med* 32:1067, 1991c.

Gilland DR, Jaszczak RJ,Liang Z,Greer KL,Coleman RE: Quantitative SPECT brain imaging: effects of attenuation and collimator response. *Conference Record of the 1991 IEEE Nuclear Science Symposium*, 1992, in press.

Greer KL, Harris CC,Jaszczak RJ,Coleman RE,Hedlund LW,Floyd CE,Manglos SH: Transmission computed tomography data acquisition with a SPECT system. *J Nucl Med Tech* 15:53-56, 1987.

Gullberg GT, Huesman RH,Malko JA,Pelc NJ,Budinger TF: An attenuated projector-backprojector for iterative SPECT reconstruction. *Phys Med Biol* 30:799-815, 1985.

Halpern SE, Haindl W,Beauregard J: Scintigraphy with In-111 labeled monoclonal antitumor antibodies. *Radiology* 168:529-536, 1988.

Hoffman EJ, Cutler PD, Digby WM, Mazziotta, JC: 3-D Phantom to simulate cerebral blood flow and

metabolic images for PET. *IEEE Trans Nucl Sci* 37:616-620, 1990.

Hubbel JH: Photon cross sections, attenuation coefficients, and energy absorption coefficients from 10 keV to 100 GeV. *Nat Stand Ref Data* 29:1969.

Jaszczak RJ, Coleman RE,Whitehead FR: Physical factors affecting quantitative measurements using camera-based single photon emission computed tomography. NS-28:69-80, 1981.

Jaszczak RJ, Greer KL,Floyd CE,Harris CC,Coleman RE: Improved SPECT quantification using compensation for scattered photons. *J Nucl Med* 25:893-900, 1984.

Jaszczak RJ, Li J,Wang H,Coleman RE: Three dimensional SPECT reconstruction of combined cone beam and parallel beam data. *Phys Med Biol* 36:1992, in press.

Jaszczak RJ, Murphy PH,Huard D,Burdine JA: Radionuclide emission computed tomography of the head with TC-99m and a scintillation camera. *J Nucl Med* 18:383-380, 1977.

Kearfott KJ, Hill SE: Simulated annealing image reconstruction method for a pinhole aperture single photon emission computed tomograph. *IEEE Trans Med Imag* 9:128-143, 1990.

King MA, Schwinger RB,Penny BC,Dohertry PW,Bianco JA: Digital restoration of indium-111 and iodine-123 SPECT images with optimized Metz filters. *J Nucl Med* 27:1327-1336, 1986.

Lange K, Carson R: EM reconstruction algorithms for emission and transmission tomography. *J Comp Assist Tomog* 8:306-316, 1984.

Lim CB, Chang LT,Jaszczak RJ: Performance analysis of three camera configurations for single photon emission computed tomography. *IEEE Trans Nucl Sci* NS-27:1137-1153, 1980.

Ljungberg M: Development and evaluation of attenuation and scatter correction techniques for SPECT using the Monte Carlo Method. *Ph.D.Dissertation,University of Lund,Sweden* 1990.

Manglos SH, Bassano DA,Thomas FD: Cone beam transmission computed tomography for nonuniform attenuation compensation of SPECT images. *J Nucl Med*, 32:1813-1820, 1991.

Manglos SH, Jaszczak RJ,Floyd CE,Hahn LH,Greer KL,Coleman RE: Nonisotropic attenuation in SPECT: Phantom test of quantitative effects and compensation techniques. *J Nucl Med* 28:1584-1591, 1987.

Metz CE: A mathematical investigation of radioisotope scan image processing. *Ph.D. Dissertation, University of Pennsylvania*, 1969.

Munley MT, Floyd CE,Tourassi GD: Out of plane photons in SPECT. *IEEE Trans Nucl Sci* 38:776-779, 1991.

Olsson LE, Ahlgren L: Tomographic scintigraphy using a pinhole collimator and a rotating gamma camera. *Nucl Med* 29:47-50, 1990.

Palmer J, Wollmer P: Pinhole emission computed tomography: method and experimental evaluation. *Phys Med Biol* 35:339-350, 1990.

Pelizzari C, Chen G,Spelbring D,Weichselbaum R,Chen CT: Accurate 3D registration of CT, PET, and/or MRI images of the brain. *J Com As Tom* 13:20-26, 1989.

Perkins AC, Primm MV: Difference in Tumour and normal tissue concentrations of iodine- and indium labeled monoclonal antibodies. *Eur J Nucl Med* 11:295-299, 1985.

Pouliot N, Gagnon D,Laperriere L,Gregoire J,Arsenault A: Maximum likelihood positioning in the scintillation camera using depth of interaction. *Conference Record of the 1991 IEEE Nuclear Science Symposium,* 1992, in press.

Rogers WL, Clinthorne NH,Stamos J: Performance evaluation of SPRINT, a single photon ring tomograph of brain imaging. *J Nucl Med* 25:1013-1018, 1984.

Rowe RK, Barrett HH,Chen J,Hall JN,Klein WP,Moore BA,Pang W,Patton DD,White TA: A stationary 3D SPECT brain imaging system. *J Nucl Med* 32:1135, 1991.

Shepp LA, Vardi Y: Maximum likelihood reconstruction for emission tomography. *IEEE Trans Med Imag* MI-1:113-122, 1982.

Smith MF, Floyd CE,Jaszczak RJ,Coleman RE: Three dimensional photon detection kernels and their application to SPECT reconstruction. *Phys Med Biol,* 1992, in press.

Thomas SR, Maxon HR,Kereiakes JG,Saenger EL: Quantitative external counting techniques enabling improved diagnostic and therapeutic decisions in patients with well-differentiated thyroid cancer. *Radiology* 122:731-737, 1977.

Tung CH, Gullberg GT,Zeng GL,Christian PE,Datz FL,Morgan HT: Nonuniform attenuation correction using simultaneous transmission and emission converging tomography. *Conference Record of the 1991 IEEE Nuclear Science Symposium,* 1992, in press.

Turkington TG, Jaszczak RJ,Greer KL,Coleman RE: Quantitation of Indium 111 activity in SPECT. *J Nucl Med* 32:986, 1991a.

Turkington TG, Jaszczak RJ,Pelizzari CA,Harris CC,MacFall JR,Hoffman JM: Measurement of accuracy in registration of PET and SPECT brain images to MR images. *Radiology* 181:186, 1991b.

Turkington TG, Jaszczak RJ, Greer KL, Coleman RE: Correlation of SPECT images of three-dimensional brain phantom using a surface fitting technique. In: *Conference Record of the 1991 IEEE Nuclear Science Symposium,* 1992a, in press.

Turkington TG, Jaszczak RJ,Hoffman JM,MacFall JR,Harris CC,Kilts CD,Pelizzari CA,Coleman RE: Accuracy of surface fit registration of PET and MR brain images. *Society of Nuclear Medicine 39th Annual Meeting,Los Angeles,June* 1992b.

van Reenen O, Lotter MG,du P.Heyns A: Quantification of the distribution of In-111 labeled platelets in organs. *Eur J Nucl Med* 7:80-84, 1982.

van Rensburg AJ, Lotter MG,du Heyns: An evaluation of four methods of In-111 planar image quantification. *Med Phys* 15:853-861, 1988.

Wang H, Jaszczak RJ,Coleman RE: Solid geometry based object model for Monte Carlo simulated emission and transmission tomographic imaging systems. *IEEE Trans Med Imaging* 1992a, in press.

Wang H. Jaszczak RJ,Gilland DR,Greer KL,Coleman RE: Solid geometry based modeling of non-uniform attenuation and Compton scattering in objects for SPECT imaging systems. *Conference Record of the 1991 IEEE Nuclear Science Symposium* 1992b, in press.

Wessels P, du P Heynes A,Pieters H: An improved method for the quantification of the in vivo kinetics of a representative population of In-111 labeled human platelets. *Eur J Nucl Med* 10:522-527, 1985.

Wu RK, Siegel JA: Absolute quantification of radioactivity using the buildup factor. *Med Phys* 11:189, 1984.

Yeh SDJ, Larson SM,Burch L,Kushner BH,Laquaglia M,Finn R,Cheung NKV: Radioimmunodetection of neuroblastoma with iodine-131-3F8. *J Nucl Med* 32:769-776, 1991.

N. APPENDICES

APPENDIX N.1.: FIGURES WITH ORIGINAL PHOTOGRAPHS

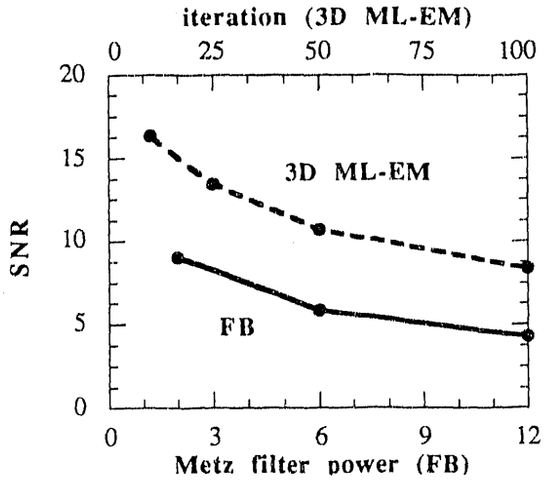

(a) On axis lesion

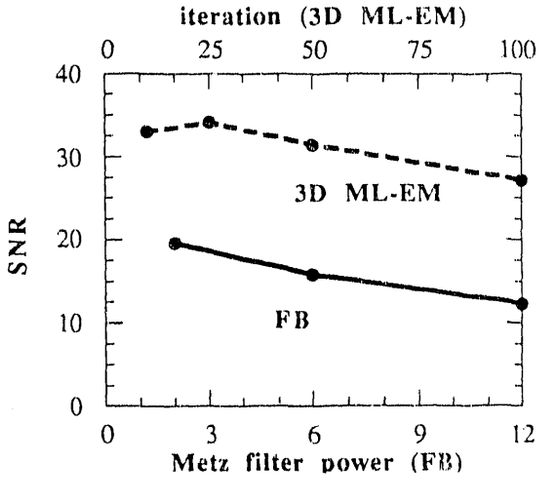

(b) Off axis lesion

Figure 1. Signal-to-noise measurements in reconstructed images

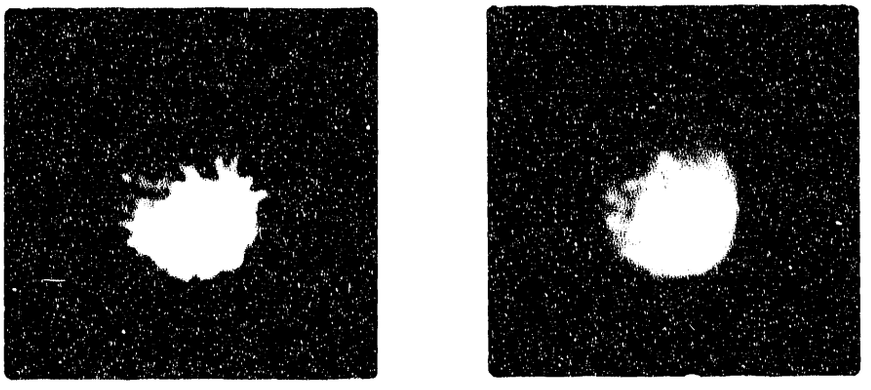

Figure 2. Reconstructed scatter data for hot lesion image. FBP is at left and ML-EM is at right.

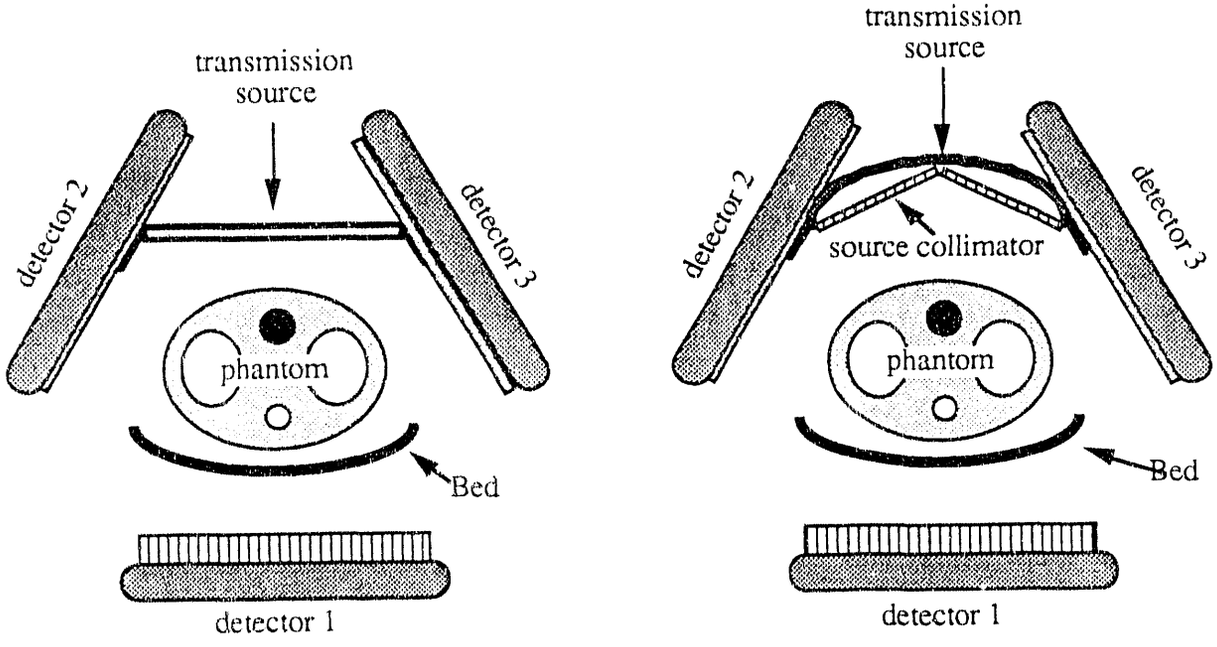

Figure 3. Transmission data acquisition using a flat transmission source (above left) and a curved transmission source with collimator (right) . Photograph of curved source is shown at bottom.

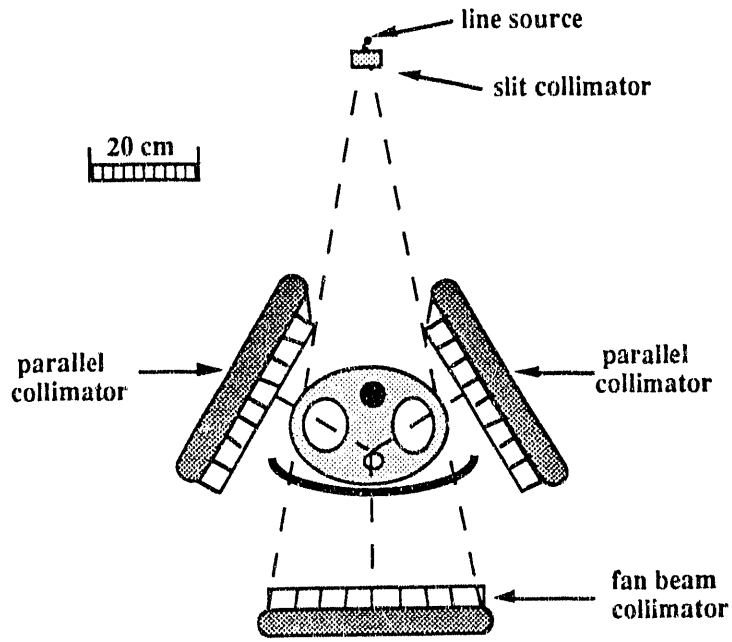

Figure 4. Sketch (top) and photograph (bottom) of line source/slit collimator for fan beam transmission CT. The bottom camera is used to acquire TCT data, while the other two cameras can be used to simultaneously acquire SPECT data.

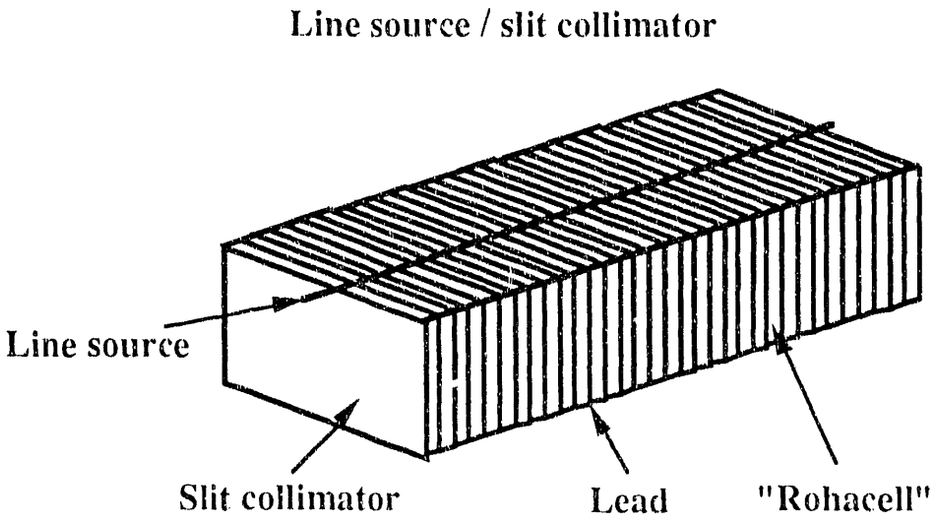

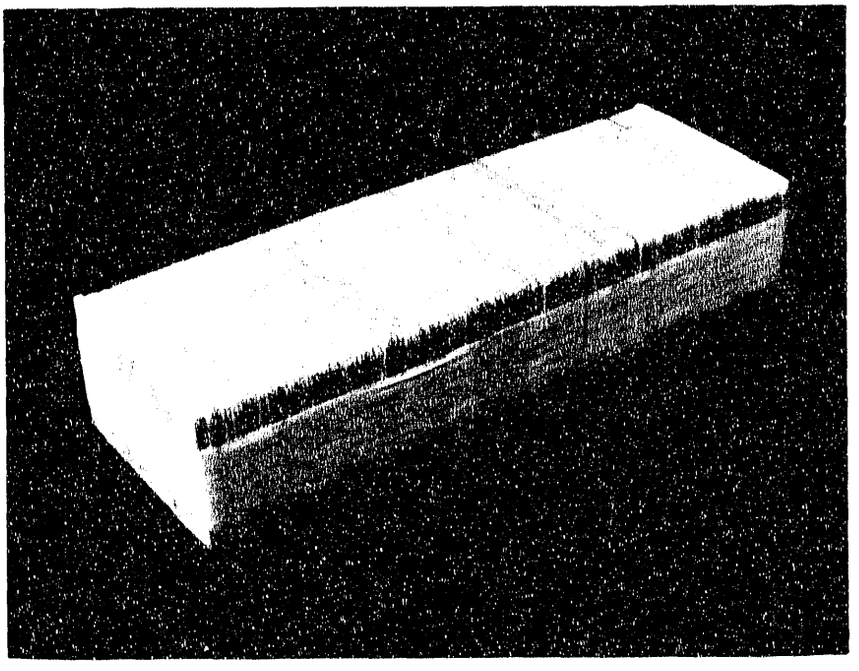

Figure 5. Sketch (top) of transmission line source/slit collimator assembly for fan beam transmission CT. Photograph (bottom) of slit collimator. The slit collimator consists of alternating layers of lead foil (0.25 mm) and Rohacell® (3.2 mm), which is a special "photon transparent" foam having highly uniform thickness.

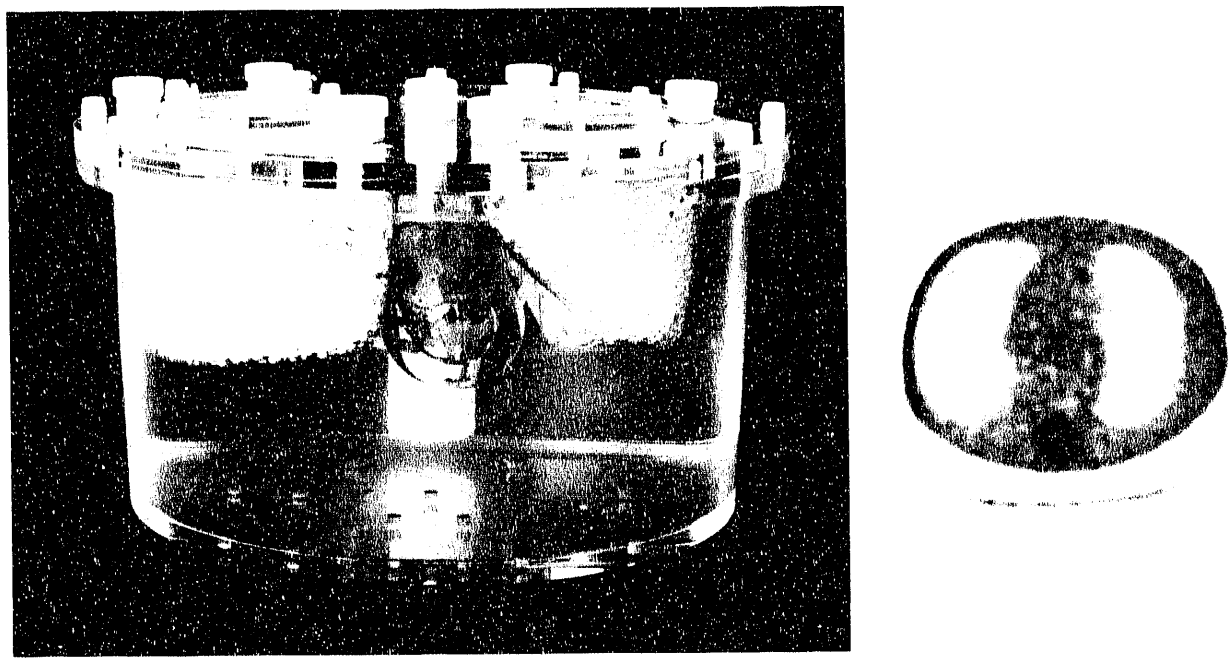

Figure 6. Photograph (left) of lung-heart phantom of a simulated thorax. Reconstructed fan beam TCT image (right) of experimentally acquired data of lung-heart phantom.

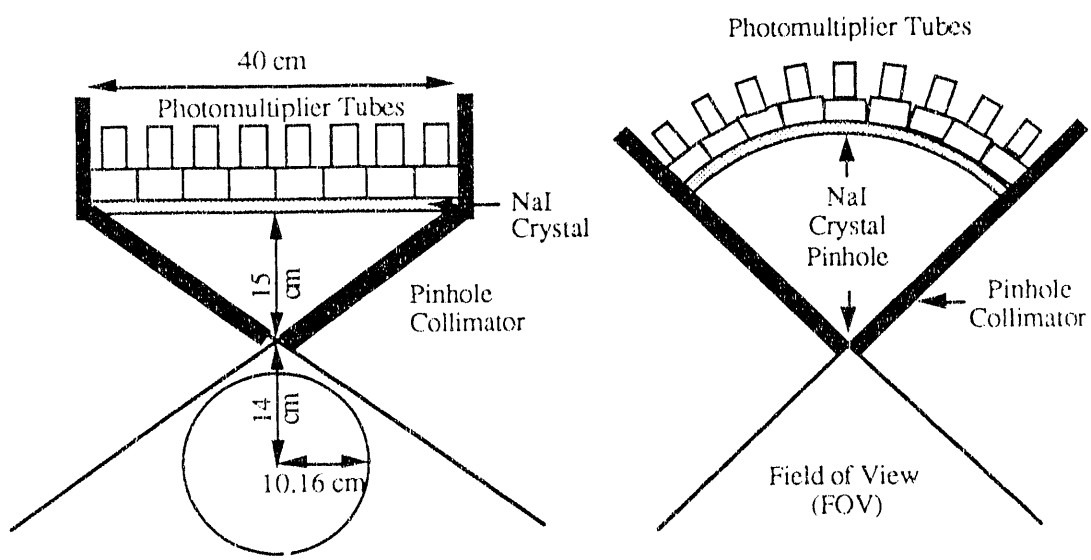

Figure 7. SPECT geometry for brain MoAb imaging using a flat (left) and a concave, spherical (right) NaI crystal.

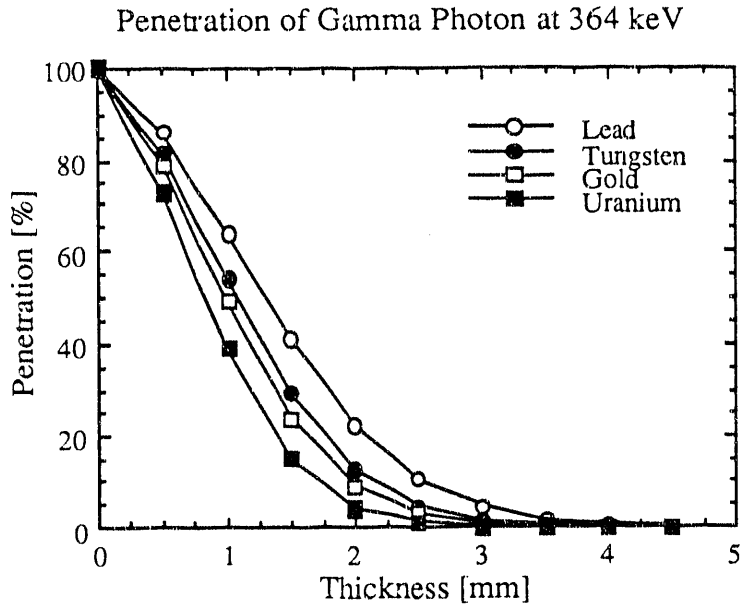

Figure 8. Penetration of 364 keV gamma rays through Pb, W, Au, and U.

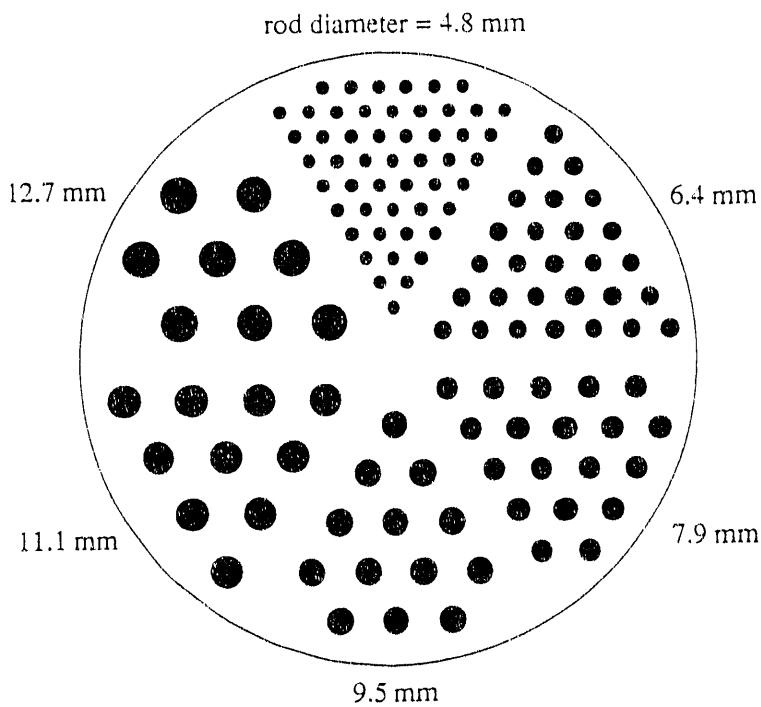

Figure 9. Sketch of "hot rod" phantom that was modeled using Monte Carlo simulations to obtain pinhole geometry SPECT projection data.

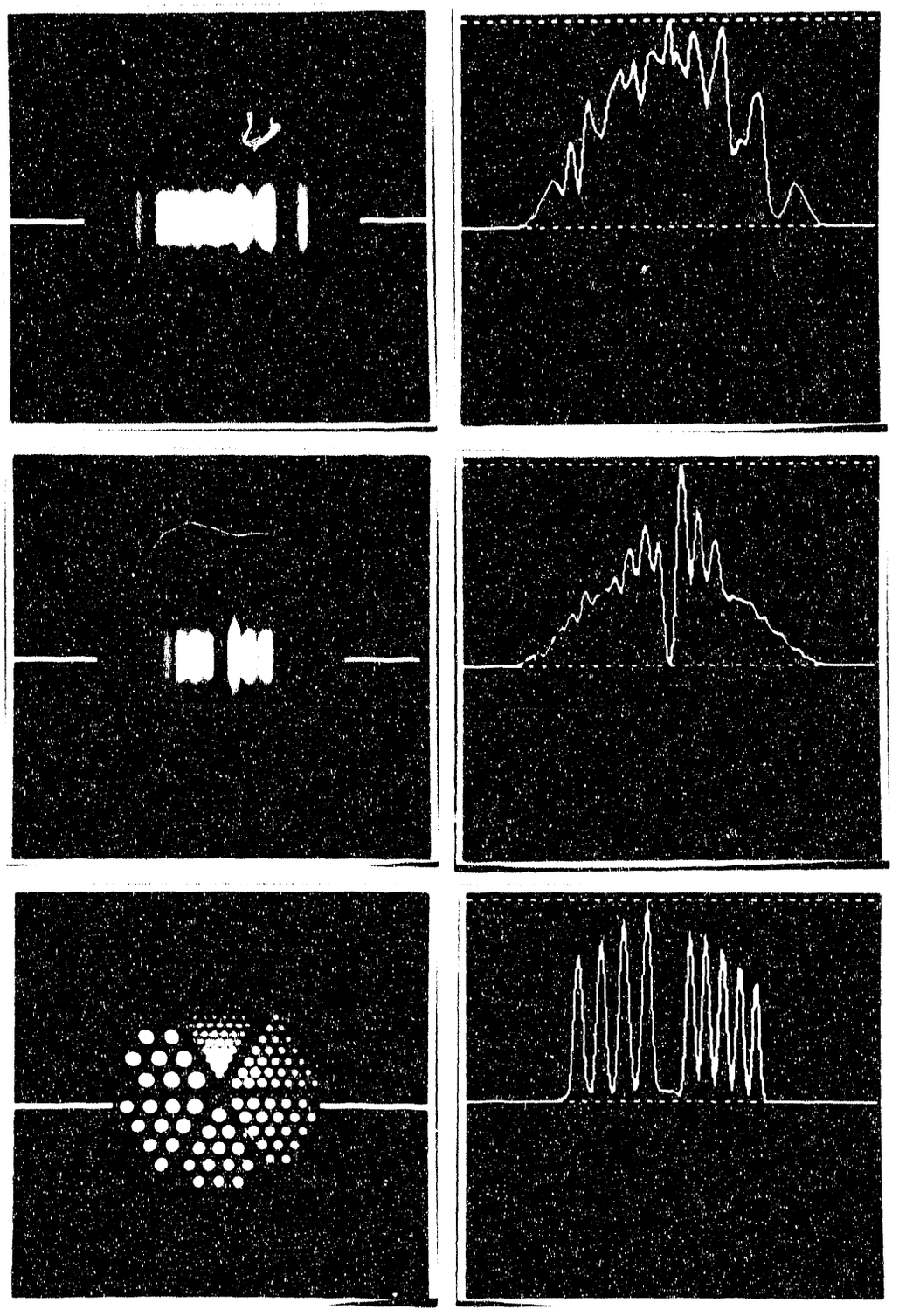

Figure 10. Sample pinhole geometry simulated projections (top 2 rows) and reconstructed transaxial image (bottom row) of hot rod phantom.

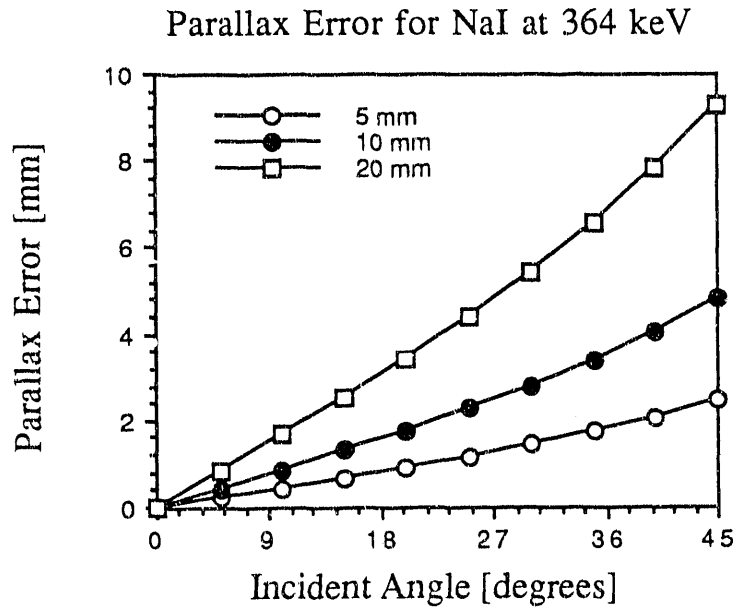

Figure 11. Parallax error as a function of thickness and angle of incidence.

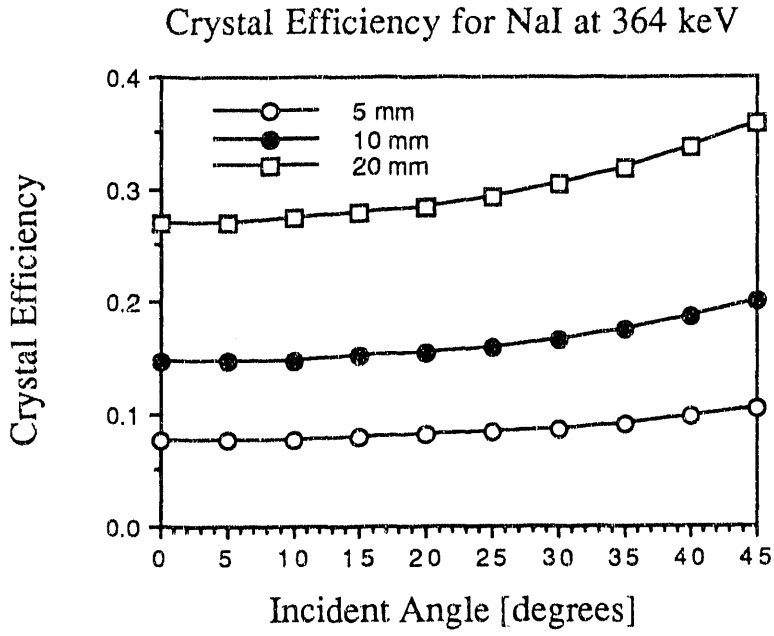

Figure 12. Efficiency of NaI crystal for 364 keV gamma rays.

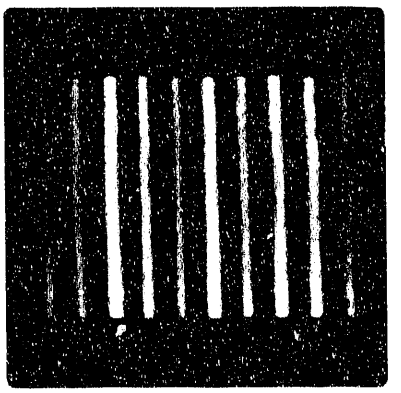

Figure 13. Composite line source image from one collimator.

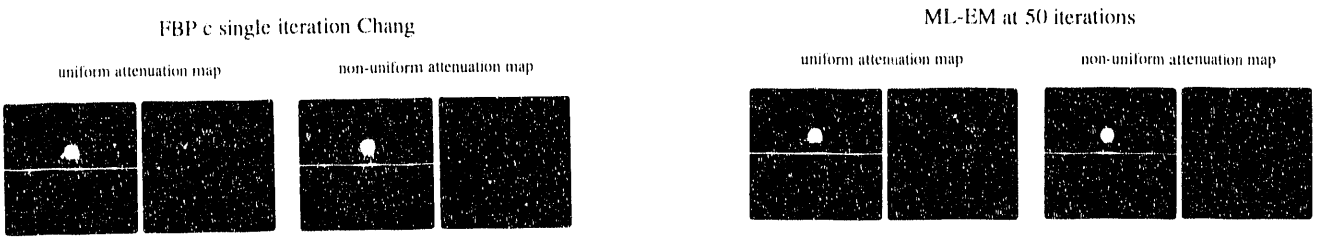

Figure 14. Filtered backprojection (left) and ML-EM (right) reconstructions with uniform and non-uniform attenuation compensation.

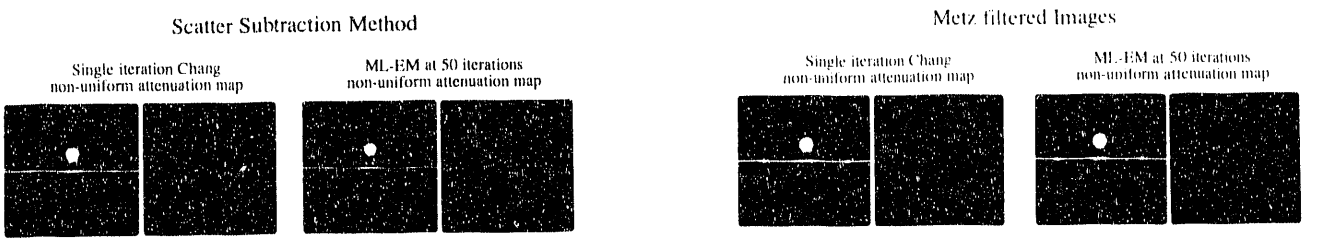

Figure 15. Scatter subtraction method (left) and Metz filter (right) applied to filtered backprojection/Chang and ML-EM reconstructions.

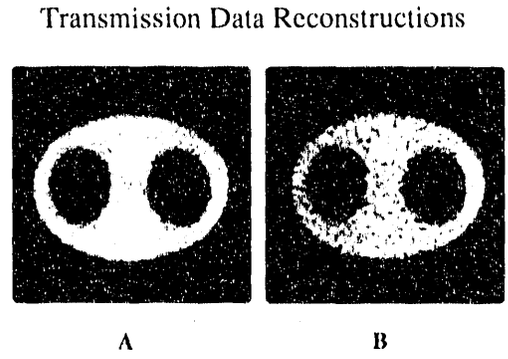

Figure 16. Reconstructed transmission data at four slice (left) and single slice (right) thickness.

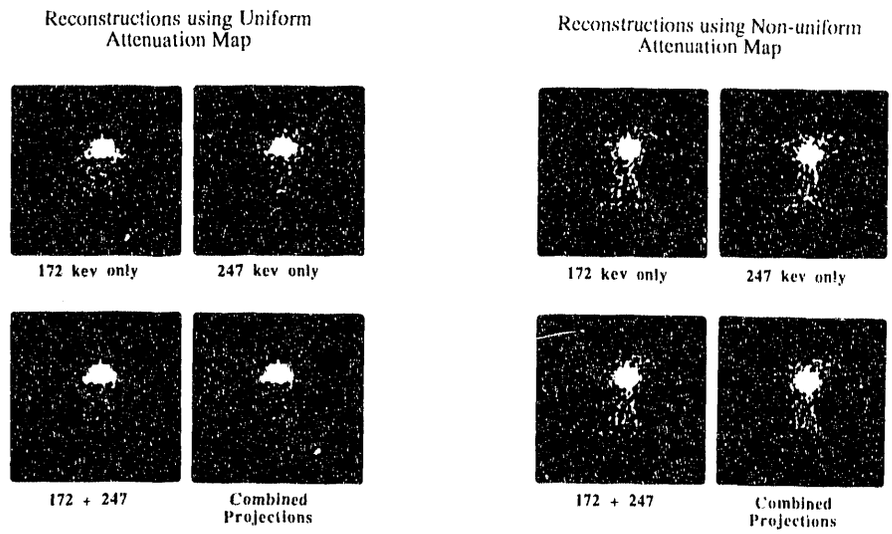

Figure 17. Uniform (left) and non-uniform (right) attenuation compensated reconstructions.

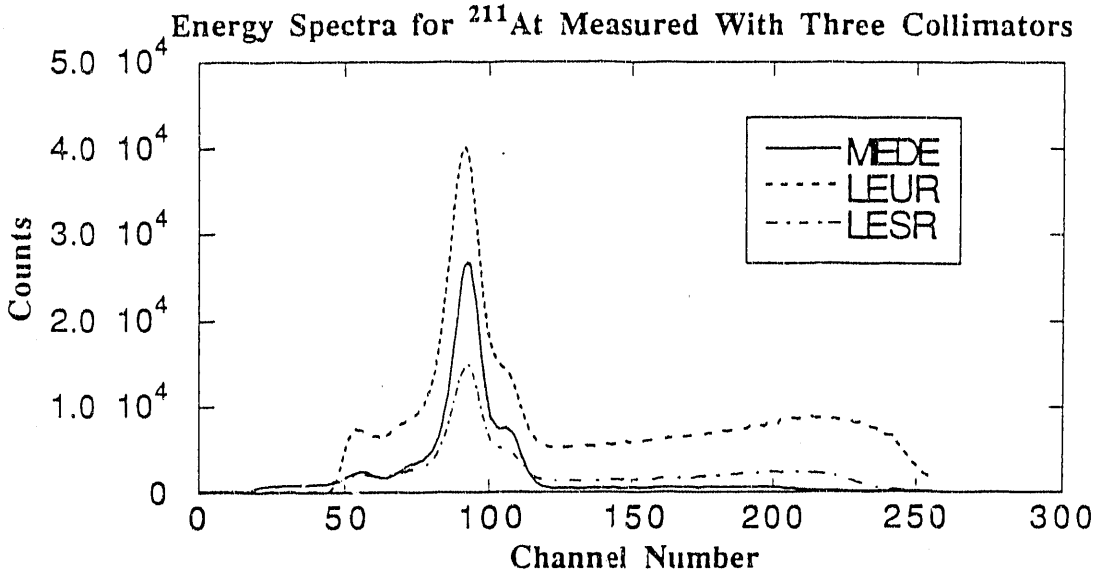

Figure 18. Energy spectra for ^{211}At with three collimators.

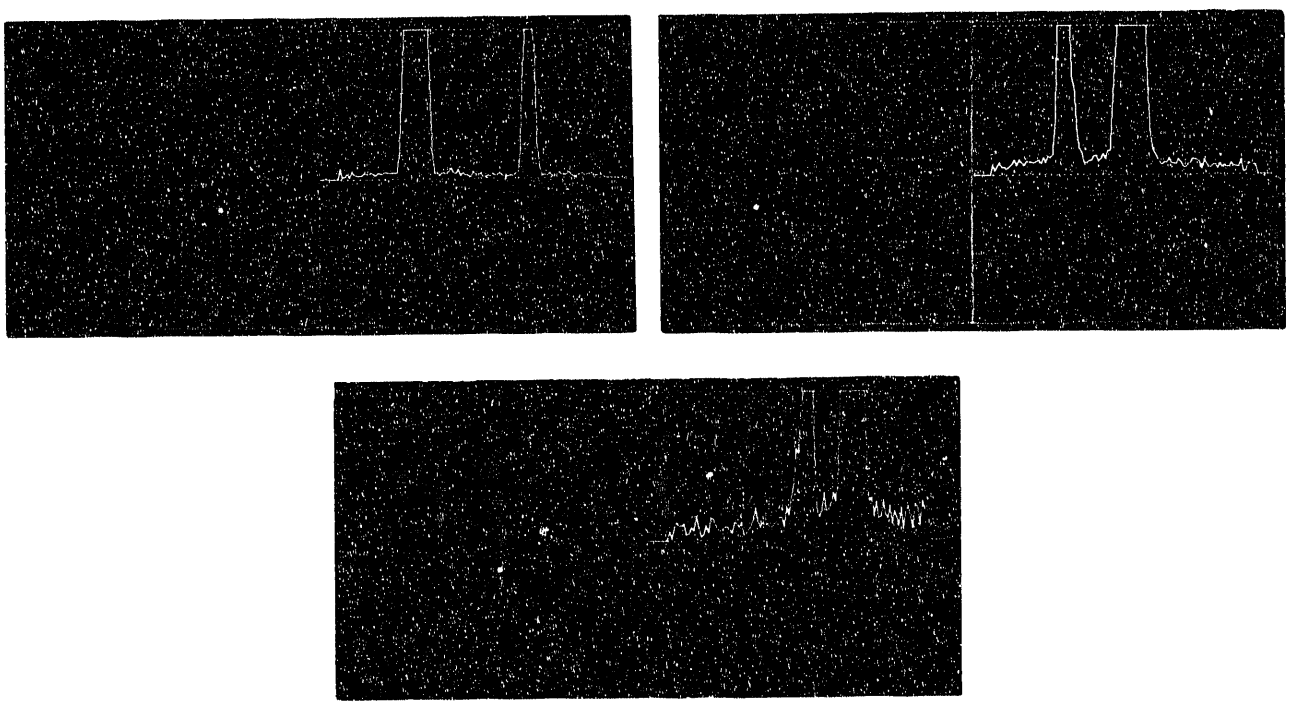

Figure 19. Projection images (different angles are shown) of ^{211}At point source and 30 ml sphere for MEDE (above left), LEUR (above right) and LESR (lower). Only the lowest 20% of profiles is shown.

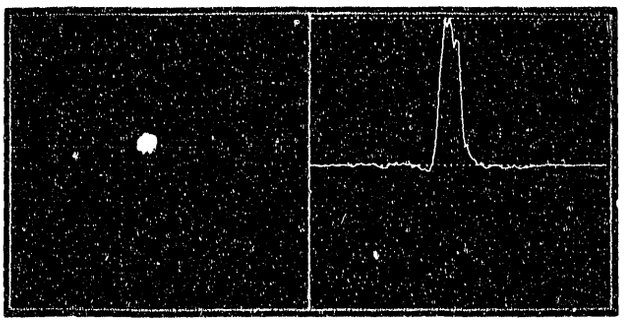

Figure 20. Reconstructed central slice with profile of 30 ml sphere in water with 200 μCi ^{211}At .

APPENDIX N.2.: SELECTED REPRINTS AND PREPRINTS

1. Gilland DR, Jaszczak RJ, Greer KL, Coleman RE: Quantitative SPECT reconstruction of iodine-123 Data. J Nucl Med 32:527-533, 1991a.

2. Gilland DR, Jaszczak RJ, Turkington TG, Greer KL, Coleman RE: Quantitative SPECT imaging with indium-111. IEEE Trans Nucl Sci 38:761-766, 1991b.

3. Gilland DR, Jaszczak RJ, Liang Z, Greer KL, Coleman RE: Quantitative SPECT brain imaging: Effects of attenuation and collimator response. IEEE Trans Nucl Sci, submitted, 1992.

4. Gilland DR, Jaszczak RJ, Greer KL, Coleman RE: SPECT quality control: Generation and reduction of artifacts. In: *Proceedings of the SE Chapter of the Society of Nuclear Medicine,* in press, 1992.

5. Turkington TG, Jaszczak RJ, Greer KL, Coleman RE: Correlation of SPECT images of a three-dimensional brain phantom using a surface fitting technique. IEEE Trans Nucl Sci, submitted, 1992.

6. Jaszczak RJ, Hoffman DC, DeVito RP: Variance propagation for SPECT with energy-weighted acquisition. In: *Conference Record of the 1990 IEEE Nuclear Science Symposium* (Arlington, VA, Dibler, 1990), pp. 1163-1171.

7. Jaszczak RJ: SPECT: State-of-the-art scanners and reconstruction strategies. In: *Radiopharmaceuticals and Brain Pathology Studied with PET and SPECT.* Ed. M. Diksic and R.C. Reba (CRC Press, 1990), pp. 93-118.

8. Jaszczak RJ, Li J, Wang H, Greer KL, Coleman RE: Three dimensional reconstruction of combined cone beam and parallel beam data. Phys Med Biol, in press, 1992.

9. Bowsher JE, Gilland DR, Floyd CE, Jaszczak RJ, Johnson VE, Coleman RE: Three-dimensional iterative reconstruction for SPECT. Society of Nuclear Medicine 39th Annual Meeting(Abstract), Los Angeles, June 1992, (Abstract) accepted (Selected as one of six finalist papers for SNM Young Investigators Award Session at SNM Annual Meeting to be held in Los Angeles, June, 1992).

10. Gilland DR, Jaszczak RJ, Turkington TG, Greer KL, Coleman RE: Transmission data acquisition with a three headed SPECT system. Society of Nuclear Medicine 39th Annual Meeting(Abstract), Los Angeles, June 1992, (Abstract) accepted.

11. Gilland DR, Bowsher JE, Jaszczak RJ, Coleman RE: Improved signal-to-noise with 3D ML-EM reconstruction. Society of Nuclear Medicine 39th Annual Meeting(Abstract), Los Angeles, June 1992, (Abstract) accepted.

12. Turkington TG, Jaszczak RJ, Hoffman JM, MacFall JR, Harris CC, Kilts CD, Pelizzari CA, Coleman RE: Accuracy of surface fit registration of PET and MR brain images. Society of Nuclear Medicine 39th Annual Meeting(Abstract), Los Angeles, June 1992, (Abstract) accepted.

13. Jaszczak RJ, Li J, Wang H, Coleman RE: SPECT collimation having spatially variant focusing (SVF). Society of Nuclear Medicine 39th Annual Meeting(Abstract), Los Angeles, June 1992, (Abstract) accepted.

Reprints + Preprints removed

END

DATE
FILMED
9 / 28 / 92